Reducing sensors for transient heat transfer problems by means of variational data assimilation

Amina Benaceur

An inexpensive Parametrized Background Data-Weak approach for time-dependent problems*

Amina Benaceur[†‡§]

Abstract

We propose a contribution that combines model reduction with data assimilation. A dedicated Parametrized Background Data-Weak (PBDW) [1] approach has been introduced in the literature so as to combine numerical models with experimental measurements. We extend the approach to a time-dependent framework by means of a `POD-greedy` reduced basis construction. Since the construction of the basis is performed offline, the algorithm addresses the time dependence of the problem while the time stepping scheme remains unchanged. Moreover, we devise a new algorithm that exploits offline state estimates in order to diminish both the dimension of the online PBDW statement and the number of required sensors collecting data. The idea is to exploit *in situ* observations in order to update the best-knowledge model, thereby improving the approximation capacity of the background space.

1 Introduction

State estimation is a task in which the quantity of interest is the 'true' state u^{true} of a physical system over a space or space-time domain of interest. However, numerical prediction based on a given mathematical model may be deficient due to limitations imposed by available knowledge. In other words, the mathematical model can only take anticipated or parametric uncertainty into account. A more accurate prediction requires the incorporation of experimental observations in order to accommodate unanticipated or non-parametric uncertainty.

The Parameterized-Background Data-Weak (PBDW) formulation for variational data assimilation is a data-driven reduced order modeling approach that was initially devised in [1] so as to merge prediction by model with prediction by data. The PBDW approach has been developed in order to estimate the true state u^{true} for several configurations of a physical system. Supposing that the true state u^{true} depends on some unknown parameter ω in an unknown parameter set Θ that represents the unanticipated uncertainty, the goal is to account for the dependency of the true state $u^{\text{true}}(\omega)$ on uncertain parameters by means of the sole knowledge of data. In this paper, whenever the context is unambiguous, the parameter ω is dropped.

The formulation combines a so-called 'best-knowledge' (`bk`) model represented by a parametrized partial differential equation (PDE) and experimentally observable measurements. The use of data in the PBDW approach is fundamental not only to reconstruct the quantities of interest, but also to correct the possible bias in the mathematical `bk` model. The PBDW approach provides the following attractive features:

*This work is partially supported by Electricité De France (EDF) and a CIFRE PhD fellowship from ANRT.

[†]University Paris-Est, CERMICS (ENPC), 77455 Marne la Vallée Cedex 2 and INRIA Paris, 75589 Paris, France.

[‡]EDF Lab Les Renardières, 77250 Ecuelles Cedex, France.

[§]Massachusetts Institute of Technology, Cambridge, USA.

The author is thankful to A. T. Patera, A. Ern and V. Ehrlacher for proof-reading and stimulating discussions.

- The PBDW variational formulation simplifies the construction of *a priori* error estimates which can guide the optimal choice of the experimental observations.

- The PBDW formulation uses a `bk` model that accommodates anticipated uncertainty associated with the parameters of the model in a computationally convenient way. This `bk` model is typically built using model-order reduction techniques.

Note that the PBDW formulation does not explicitly include the equations of the `bk` model, but only a finite collection of solutions to the `bk` model. Thus, another important feature of the PBDW approach is its non-intrusiveness. In fact, once the subspace $\mathcal{Z}_N$ has been generated, we no longer need the `bk` model.

The PBDW approach has been subject to active research in recent years. It has been used for several applications. For instance, [2] applies the PBDW for structural health monitoring; [3] proposes a non-intrusive PBDW with application to urban dispersion modeling frameworks; and [4, 5] exploit the generalized empirical interpolation method [6, 7, 8] for efficient sensor placement in nuclear reactors. As a further step towards efficient industrial implementation, [9] develops a PBDW approach based on noisy observations and [10] introduces an adaptive PBDW approach with a user-defined update space. Moreover, [11] tackles the case of nonlinear problems, which is coupled with the additional issue of noisy observations in [12]. Further work regarding the selection of experimental observation functionals has been conducted in [13], whereas [14] proposes a localization procedure that treats the uncertainty related to boundary conditions. Finally, [15] proposes optimal choices for the reduced models and [16] addresses optimal measurements in state estimation using reduced models.

The PBDW approach was devised in [1] for steady problems. To our knowledge, the related research in the literature remains in the steady framework. In this paper, we propose, as initiated in [17], an extension of the PBDW approach to time-dependent state estimation. Two main contributions to the standard PBDW approach are presented:

- We build appropriate background spaces for the time-dependent setting using the `POD-greedy` algorithm [18].

- We propose a modified offline stage so as to alleviate its computational cost which can be sizable in a time-dependent setting. The new offline stage allows for a better computational efficiency owing to a smaller online system. Moreover, it achieves substantial cost savings associated with data collection since it diminishes the number of observation sensors needed online. Note that this modified offline stage can also be applied to a steady framework.

This paper is organized as follows. In Section 2, we set the notation and recall the standard PBDW approach for steady problems as introduced in [1]. The reader familiar with the material can skip this section and jump directly to Section 3, where we extend the PBDW approach to the time-dependent framework. In Section 4, we discuss the offline stage and present the suggested algorithm in detail. Finally, in Section 5, we illustrate our method by numerical results.

2 Parametrized-Background Data-Weak (PBDW) approach

In this section, we first introduce the notation that will be used throughout the paper. Here, we focus on a time-independent setting. We consider a spatial domain (open, bounded, connected subset) $\Omega \subset \mathbb{R}^d$, $d \geqslant 1$, with a Lipschitz boundary. We introduce a Hilbert space $\mathcal{U}$ composed of functions defined over Ω. The space $\mathcal{U}$ is endowed with an inner product $(\cdot, \cdot)$ and we denote by $\|\cdot\|$ the induced norm; $\mathcal{U}$ consists of functions $\{w : \Omega \to \mathbb{R} \mid \|w\| < \infty\}$. To fix the ideas, we assume that $H_0^1(\Omega) \subset \mathcal{U} \subset H^1(\Omega)$, and we denote the dual space of $\mathcal{U}$ by $\mathcal{U}'$. The Riesz operator $R_{\mathcal{U}} : \mathcal{U}' \to \mathcal{U}$

satisfies, for each $\ell \in \mathcal{U}'$, and for all $v \in \mathcal{U}$, the equality $(R_{\mathcal{U}}(\ell), v) = \ell(v)$. For any closed subspace $\mathcal{Q} \subset \mathcal{U}$, the orthogonal complement of $\mathcal{Q}$ is defined as $\mathcal{Q}^{\perp} := \{w \in \mathcal{U} \mid (w, v) = 0, \ \forall v \in \mathcal{Q}\}$. Finally, we introduce a parameter set $\mathcal{P} \subset \mathbb{R}^p, \ p \geqslant 1$, whose elements are generically denoted by $\mu \in \mathcal{P}$.

2.1 Best-knowledge (bk) model

The first source of information we shall afford ourselves in the PBDW approach is a so-called 'best-knowledge' (bk) mathematical model in the form of a parameterized PDE posed over the domain Ω (or more generally, over a domain Ω^{bk} such that $\Omega \subset \Omega^{\text{bk}}$). Given a parameter value μ in the parameter set $\mathcal{P}$, we denote the solution to the bk parameterized PDE as $u^{\text{bk}}(\mu) \in \mathcal{U}$. Then, we introduce the manifold associated with the solutions of the bk model $\mathcal{M}^{\text{bk}} := \{u^{\text{bk}}(\mu) \mid \mu \in \mathcal{P}\} \subset \mathcal{U}$. In ideal situations, the true solution u^{true} is well approximated by the bk manifold, i.e., the model error

$$\epsilon^{\text{bk}}_{\text{mod}}(u^{\text{true}}) := \inf_{z \in \mathcal{M}^{\text{bk}}} \|u^{\text{true}} - z\|, \tag{1}$$

is very small.

We introduce nested background subspaces $\mathcal{Z}_1 \subset \ldots \subset \mathcal{Z}_N \subset \ldots \subset \mathcal{U}$ that are generated to approximate the bk manifold $\mathcal{M}^{\text{bk}}$ to a certain accuracy. These subspaces can be built using various model-order reduction techniques, for instance, the Reduced Basis method. Note that the indices of the subspaces conventionally indicate their dimensions. To measure how well the true solution is approximated by the background space $\mathcal{Z}_N$, we define the quantity $\epsilon^{\text{bk}}_N(u^{\text{true}}) := \inf_{z \in \mathcal{Z}_N} \|u^{\text{true}} - z\|$. When N is large enough, we have $\epsilon^{\text{bk}}_N(u^{\text{true}}) \approx \epsilon^{\text{bk}}_{\text{mod}}(u^{\text{true}})$. Moreover, we introduce the reduction error $\epsilon^{\text{bk}}_{\text{red},N} := \sup_{u \in \mathcal{M}^{\text{bk}}} \inf_{z \in \mathcal{Z}_N} \|u - z\|$, which encodes the loss of accuracy caused by solving the bk model in the N-dimensional background space $\mathcal{Z}_N$. Figure 1 illustrates both the model and reduction errors, where $\Pi_{\mathcal{Z}_N}(u^{\text{true}})$ and $\Pi_{\mathcal{M}^{\text{bk}}}(u^{\text{true}})$ are the closest points to u^{true} in $\mathcal{Z}_N$ and $\mathcal{M}^{\text{bk}}$, respectively. Note that $\Pi_{\mathcal{Z}_N}$ is the $\mathcal{U}$-orthogonal projection onto $\mathcal{Z}_N$. The background space $\mathcal{Z}_N$ can be interpreted as a

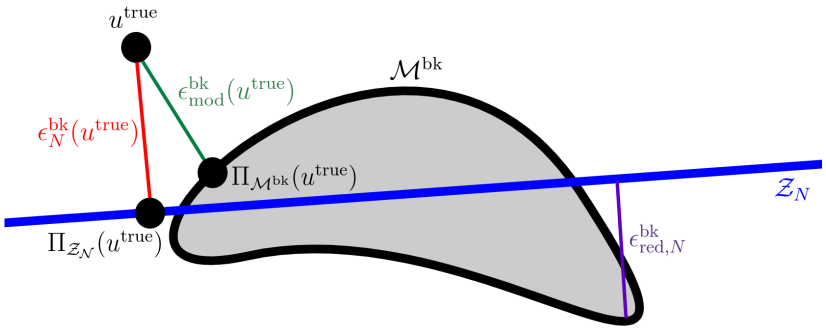

Figure 1: Model and reduction errors.

prior space that approximates the bk manifold which we hope approximates well the true state u^{true}. As previously alluded to, u^{true} rarely lies in $\mathcal{M}^{\text{bk}}$ in realistic engineering study cases.

2.2 Unlimited-observations statement

Let us first describe an ideal situation. The unlimited-observations PBDW statement reads: find $(u^*_N, z^*_N, \eta^*_N) \in \mathcal{U} \times \mathcal{Z}_N \times \mathcal{U}$ such that

$$(u^*_N, z^*_N, \eta^*_N) = \underset{\substack{u_N \in \mathcal{U} \\ z_N \in \mathcal{Z}_N \\ \eta_N \in \mathcal{U}}}{\text{arginf}} \|\eta_N\|^2, \tag{2}$$

subject to

$$(u_N, v) = (\eta_N, v) + (z_N, v), \quad \forall v \in \mathcal{U}, \tag{3a}$$
$$(u_N, \phi) = (u^{\text{true}}, \phi), \quad \forall \phi \in \mathcal{U}. \tag{3b}$$

A direct consequence of (3a) is that

$$u_N^* = z_N^* + \eta_N^*, \tag{4}$$

whereas (3b) implies that $u_N^* = u^{\text{true}}$. We will be using the following terminology:

- **State estimate:** The goal of the PBDW statement (2)-(3) being to estimate the true state u^{true}, the first component of its solution, u_N^*, is called the 'state estimate'. In the present ideal situation of unlimited observations, the state estimate coincides with the true state.
- **Deduced background estimate:** The first contribution z_N^* in (4) lies in the background space $\mathcal{Z}_N$ and is deduced from the PBDW statement, which takes the observations into account. Hence, z_N^* is called the 'deduced background estimate'.
- **Update estimate:** The second contribution η_N^* in (4) is brought by the inclusion of the observations in the PBDW statement. The observations supplement the `bk` model. Thus, η_N^* is called the 'update estimate'.

The deduced background estimate z_N^* can only represent anticipated uncertainty. Since the `bk` mathematical model of a physical system is often deficient, one cannot realistically assume that the state estimate u_N^* of u^{true} lies completely in the `bk` manifold (or in the background space $\mathcal{Z}_N$). Therefore, the update estimate η_N^* is meant to cure the deficiency of the `bk` model by capturing unanticipated uncertainty. In other words, the key idea of the PBDW statement (2) is to search for the smallest correction to the `bk` manifold. The following result is proved in [1].

Proposition 1 (Unlimited observations)**.** *The solution of* (2)-(3) *is given by*

$$u_N^* = u^{\text{true}}, \quad z_N^* = \Pi_{\mathcal{Z}_N}(u^{\text{true}}), \quad \eta_N^* = \Pi_{\mathcal{Z}_N^\perp}(u^{\text{true}}). \tag{5}$$

Proof. We have already seen that $u_N^* = u^{\text{true}}$. Next, we deduce from (3a) that $u^{\text{true}} = z_N^* + \eta_N^*$. Since (2) is a minimization of $\|\eta_N^*\|$, it follows that $z_N^* = \Pi_{\mathcal{Z}_N}(u^{\text{true}})$. Thus, $\eta_N^* = \Pi_{\mathcal{Z}_N^\perp}(u^{\text{true}})$. □

The Euler–Lagrange saddle-point problem associated with the PBDW statement (2)-(3) reads: find $(z_N^*, \eta_N^*) \in \mathcal{Z}_N \times \mathcal{U}$ such that

$$\begin{cases} (\eta_N^*, q) + (z_N^*, q) = (u^{\text{true}}, q), & \forall q \in \mathcal{U}, \\ (\eta_N^*, p) = 0, & \forall p \in \mathcal{Z}_N, \end{cases} \tag{6}$$

and set $u_N^* = z_N^* + \eta_N^*$.

As mentioned earlier, the saddle-point problem (6) is purely geometric and does not include any explicit reference to the `bk` model. The unique link to the `bk` model is through the background space $\mathcal{Z}_N$. Therefore, the PBDW approach is applicable to a wide class of engineering problems. Moreover, the non-intrusiveness of (6) simplifies its implementation.

2.3 Observable space

The evaluation of the right-hand side (u^{true}, q) in (6) requires the full knowledge of the true state u^{true} which is unrealistic. In practice, one can only afford a limited number of experimental observations of the true state u^{true}. In the present setting, the experimental observations are interpreted as the

application of prescribed observation functionals $\ell_m^{\rm obs} \in \mathcal{U}'$ for all $m \in \{1, \dots, M\}$ such that the m-th experimental observation is given by $\ell_m^{\rm obs}(u^{\rm true}) \in \mathbb{R}, \quad \forall m \in \{1, \dots, M\}$. One can consider any observation functional that renders the behavior of some physical sensor. In the case of sensors measuring the state locally over user-defined subsets $\mathcal{R}_m \subset \Omega$, where $m \in \{1, \dots, M\}$, one possibility is to model each sensor through uniform local integration

$$\ell_m^{\rm obs}(v) = \frac{1}{|\mathcal{R}_m|} \int_{\mathcal{R}_m} v(x) dx, \quad \forall v \in \mathcal{U}. \tag{7}$$

Another plausible option is, as introduced in [1], to consider

$$\ell_m^{\rm obs}(v) = \frac{1}{\sqrt{2\pi r_m^2}} \int_{\mathcal{R}_m} v(x) \exp\left(\frac{-(x - x_m^c)^2}{2r_m^2}\right) dx, \tag{8}$$

where x_m^c is the center of the Gaussian that reflects the location of the sensor, and $r_m \ll |\mathcal{R}_m|^{\frac{1}{d}}$ is the standard deviation of the Gaussian that reflects the filter width of the sensor.

Generally, we introduce an experimentally observable space $\mathcal{U}_M := \text{Span}\{q_m\}_{1 \leqslant m \leqslant M} \subset \mathcal{U}$, where $q_m := R_{\mathcal{U}}(\ell_m^{\rm obs})$ is the Riesz representation of $\ell_m^{\rm obs} \in \mathcal{U}'$, for all $m \in \{1, \dots, M\}$. The experimental observations of the true state satisfy $(u^{\rm true}, q_m) = \ell_m^{\rm obs}(u^{\rm true})$, for all $m \in \{1, \dots, M\}$. Hence, for all $q \in \mathcal{U}_M$ such that $q = \sum_{m=1}^M \alpha_m q_m$ and $(\alpha_m)_{1 \leqslant m \leqslant M} \in \mathbb{R}^M$, the inner product $(u^{\rm true}, q)$ can be deduced from the experimental observations as a linear combination of the M available observations:

$$\left(u^{\rm true}, q\right) = \sum_{m=1}^M \alpha_m \left(u^{\rm true}, q_m\right) = \sum_{m=1}^M \alpha_m \ell_m^{\rm obs}(u^{\rm true}). \tag{9}$$

2.4 Limited-observations statement

Let us now describe the PBDW statement in the case of limited observations. Henceforth, we make the crucial assumption that

$$\mathcal{Z}_N \cap \mathcal{U}_M^\perp = \{0\}, \tag{10}$$

which is meant to ensure the well-posedness of the PBDW statement with limited observations (cf. Proposition 3 below). This assumption can be viewed as a requirement to have enough sensors (note that $\mathcal{Z}_N \cap \mathcal{U}^\perp = \{0\}$). The limited-observations PBDW statement reads: find $(u_{N,M}^*, z_{N,M}^*, \eta_{N,M}^*) \in \mathcal{U} \times \mathcal{Z}_N \times \mathcal{U}$ such that

$$(u_{N,M}^*, z_{N,M}^*, \eta_{N,M}^*) = \underset{\substack{u_{N,M} \in \mathcal{U} \\ z_{N,M} \in \mathcal{Z}_N \\ \eta_{N,M} \in \mathcal{U}}}{\text{arginf}} \|\eta_{N,M}\|^2, \tag{11}$$

subject to

$$(u_{N,M}, v) = (\eta_{N,M}, v) + (z_{N,M}, v), \quad \forall v \in \mathcal{U}, \tag{12a}$$
$$(u_{N,M}, \phi) = (u^{\rm true}, \phi), \quad \forall \phi \in \mathcal{U}_M. \tag{12b}$$

As above, (12a) implies that the limited-observations state estimate $u_{N,M}^*$ satisfies

$$u_{N,M}^* = z_{N,M}^* + \eta_{N,M}^*. \tag{13}$$

One can show (e.g., by introducing the Lagrangian) that the limited-observations problem (11)-(12) is equivalent to the limited-observations saddle-point problem: find $(z_{N,M}^*, \eta_{N,M}^*) \in \mathcal{Z}_N \times \mathcal{U}_M$ such that

$$(\eta_{N,M}^*, q) + (z_{N,M}^*, q) = (u^{\rm true}, q), \quad \forall q \in \mathcal{U}_M, \tag{14a}$$
$$(\eta_{N,M}^*, p) = 0, \quad \forall p \in \mathcal{Z}_N, \tag{14b}$$

and define $u_{N,M}^*$ according to (13). We will see in Proposition 3 below that the linear system (14) is well posed under the assumption (10).

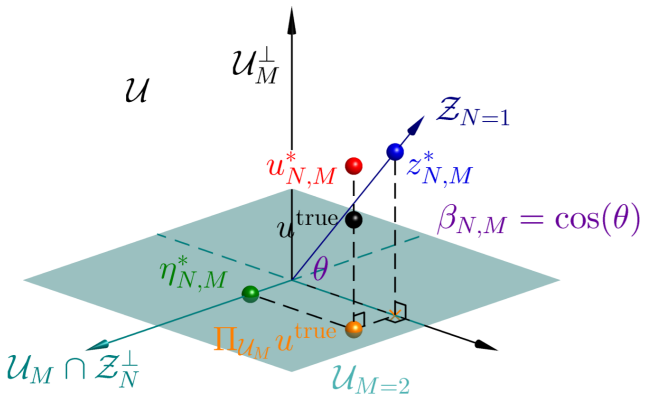

Figure 2: PBDW state estimation (courtesy of A. T. Patera).

Proposition 2 (Update estimate)**.** *The update estimate is given by*

$$\eta^*_{N,M} = \Pi_{\mathcal{Z}_N^\perp \cap \mathcal{U}_M}(u^{\text{true}}). \tag{15}$$

Proof. By definition of the saddle-point problem (14), $\eta^*_{N,M} \in \mathcal{U}_M$. From (14b), we infer that $\eta^*_{N,M} \in \mathcal{Z}_N^\perp$. Hence, $\eta^*_{N,M} \in \mathcal{Z}_N^\perp \cap \mathcal{U}_M$. Thus, we have

$$u^*_{N,M} = z^*_{N,M} + \eta^*_{N,M} \in \mathcal{Z}_N \oplus (\mathcal{Z}_N^\perp \cap \mathcal{U}_M).$$

Then, (14a) yields

$$(\eta^*_{N,M}, q) = (u^{\text{true}}, q), \quad \forall q \in \mathcal{Z}_N^\perp \cap \mathcal{U}_M.$$

We conclude that $\eta^*_{N,M} = \Pi_{\mathcal{Z}_N^\perp \cap \mathcal{U}_M}(u^{\text{true}})$. □

The decomposition of the state estimate $u^*_{N,M}$ is illustrated in Figure 2.

Remark 1 (Perfect background space)**.** *The choice of the background space $\mathcal{Z}_N$ and of the observable space $\mathcal{U}_M$ may lead to several specific configurations. In particular, the background space $\mathcal{Z}_N$ is said to be perfect if the reduction error (cf. Figure 1) vanishes, i.e., $u^{\text{true}} \in \mathcal{Z}_N$. In this case, the pair $(u^{\text{true}}, 0) \in \mathcal{Z}_N \times \mathcal{U}_M$ is the unique solution to (14). Hence, the state estimate $u^*_{N,M}$ also belongs to $\mathcal{Z}_N$ and the update estimate satisfies $\eta^*_{N,M} = 0$.*

2.5 Algebraic formulation

We now present the algebraic formulation of the limited-observations PBDW statement. We first introduce an $\mathcal{N}$-dimensional approximation space $\mathcal{U}^\mathcal{N}$ of the infinite-dimensional space $\mathcal{U}$ as well as discrete approximation spaces $\mathcal{Z}_N \subset \mathcal{U}^\mathcal{N}$ and $\mathcal{U}_M \subset \mathcal{U}^\mathcal{N}$ of the subspaces $\mathcal{Z}_N$ and $\mathcal{U}_M$, respectively. These spaces are built using the Finite Element Method (FEM) [19]. We assume that the size of the mesh is small enough that the $\mathcal{N}$-dimensional space discretization delivers High-Fidelity (HF) approximations within the requested level of accuracy. To simplify the notation, we have dropped the superscript $\mathcal{N}$; hence, the discrete FEM spaces are denoted $\mathcal{Z}_N$ and $\mathcal{U}_M$ instead of $\mathcal{Z}_N^\mathcal{N}$ and $\mathcal{U}_M^\mathcal{N}$, but we still keep the notation $\mathcal{U}^\mathcal{N}$ for the FEM-discretization space. Then, we introduce a basis for the background space $\mathcal{Z}_N := \text{Span}\{\zeta_n\}_{1 \leqslant n \leqslant N}$. The update space is spanned by the Riesz representations of the observation functionals in $\mathcal{U}^\mathcal{N}$, i.e., $\mathcal{U}_M := \text{Span}\{q_m\}_{1 \leqslant m \leqslant M}$, where $q_m \in \mathcal{U}^\mathcal{N}$, for all $m \in \{1, \dots, M\}$. The HF discretization of the saddle-point problem (14) is: Find $(z^*_{N,M}, \eta^*_{N,M}) \in \mathcal{Z}_N \times \mathcal{U}_M$ such that

$$(\eta^*_{N,M}, q) + (z^*_{N,M}, q) = (u^{\text{true}}, q), \quad \forall q \in \mathcal{U}_M, \tag{16a}$$

$$(\eta^*_{N,M}, p) = 0, \quad \forall p \in \mathcal{Z}_N. \tag{16b}$$

The solution of (16) is then searched under the form

$$z^*_{N,M} = \sum_{n=1}^{N} z_n \zeta_n, \quad \text{and} \quad \eta^*_{N,M} = \sum_{m=1}^{M} \eta_m q_m, \tag{17}$$

and we introduce the component vectors $\boldsymbol{z}^*_{N,M} := (z_n)_{1\leqslant n\leqslant N} \in \mathbb{R}^N$ and $\boldsymbol{\eta}^*_{N,M} := (\eta_m)_{1\leqslant m\leqslant M} \in \mathbb{R}^M$. We also introduce the basis matrices $\mathbf{Z}_N \in \mathbb{R}^{\mathcal{N}\times N}$ and $\mathbf{U}_M \in \mathbb{R}^{\mathcal{N}\times M}$ whose column vectors are the components of the functions $\{\zeta_n\}_{1\leqslant n\leqslant N}$ and $\{q_m\}_{1\leqslant m\leqslant M}$ respectively in the basis of $\mathcal{U}^{\mathcal{N}}$. In algebraic form, the FEM-discretized saddle-point problem (16) reads: find $(\boldsymbol{z}^*_{N,M}, \boldsymbol{\eta}^*_{N,M}) \in \mathbb{R}^N \times \mathbb{R}^M$ such that

$$\begin{pmatrix} \mathbf{A} & \mathbf{B} \\ \mathbf{B}^T & \mathbf{0} \end{pmatrix} \begin{pmatrix} \boldsymbol{\eta}^*_{N,M} \\ \boldsymbol{z}^*_{N,M} \end{pmatrix} = \begin{pmatrix} \boldsymbol{\ell}^{\mathrm{obs}}_M \\ \mathbf{0} \end{pmatrix}, \tag{18}$$

with the matrices

$$\mathbf{A} = \Big((q_{m'}, q_m)\Big)_{1\leqslant m,m'\leqslant M} \in \mathbb{R}^{M\times M}, \ \mathbf{B} = \Big((\zeta_n, q_m)\Big)_{1\leqslant m\leqslant M, 1\leqslant n\leqslant N} \in \mathbb{R}^{M\times N}, \tag{19}$$

and the vector of observations $\boldsymbol{\ell}^{\mathrm{obs}}_M = \big(\ell^{\mathrm{obs}}_m(u^{\mathrm{true}})\big)_{1\leqslant m\leqslant M} \in \mathbb{R}^M$.

Proposition 3 (Well-posedness)**.** *The PBDW statement* (18) *has a unique solution if and only if* $\mathcal{Z}_N \cap \mathcal{U}_M^\perp = \{0\}$*. Equivalently, under this assumption, the stability constant*

$$\beta_{N,M} := \inf_{w\in\mathcal{Z}_N} \sup_{v\in\mathcal{U}_M} \frac{(w,v)}{\|w\|\ \|v\|} \in (0,1]. \tag{20}$$

Proof. The system (18) is a saddle-point problem with a symmetric positive definite matrix $\mathbf{A}$. Therefore, it has a unique solution if and only if the matrix $\mathbf{B}$ is injective, i.e., if and only if $\ker(\mathbf{B}) = \{0\}$. Using the definition of $\mathbf{B}$ in (19), we have

$$\begin{aligned} \ker(\mathbf{B}) \neq \{0\} &\iff \exists z \in \mathcal{Z}_N\backslash\{0\} :\ \forall q \in \mathcal{U}_M : (z,q) = 0, \\ &\iff \mathcal{Z}_N \cap \mathcal{U}_M^\perp \neq \{0\}. \end{aligned} \tag{21}$$

Thus, (18) is well-posed if and only if $\mathcal{Z}_N \cap \mathcal{U}_M^\perp = \{0\}$ and this statement is equivalent to $\beta_{N,M} > 0$. Finally, we readily verify that $\beta_{N,M} \leqslant 1$ owing to the Cauchy–Schwarz inequality. □

Remark 2 (Stability constant)**.** *In terms of geometry, the stability constant* $\beta_{N,M}$ *is equal to the cosine of the angle between the linear subspaces* $\mathcal{Z}_N$ *and* $\mathcal{U}_M^\perp$ *(cf. Figure 2). Furthermore, it is readily verified that*

$$\beta_{N,M} = 0 \iff \mathcal{Z}_N \cap \mathcal{U}_M^\perp \neq \{0\}, \tag{22a}$$

$$\beta_{N,M} = 1 \iff \mathcal{Z}_N \subset \mathcal{U}_M. \tag{22b}$$

The case (22b) *can hardly occur in practice with a reasonable (not too high) number of observation sensors. Loosely speaking, a sensor is localized in space. Thus, it concerns only a limited number of degrees of freedom.*

Remark 3 (Insufficient observations)**.** *If* $M < N$*, then* (18) *is necessarily ill-posed. Indeed, we have*

$$M < N \iff \dim(\mathcal{U}_M) < \dim(\mathcal{Z}_N).$$

Moreover, we have

$$\begin{aligned} \dim(\mathcal{Z}_N) - \operatorname{codim}(\mathcal{U}_M^\perp) \leqslant \dim(\mathcal{Z}_N \cap \mathcal{U}_M^\perp) &\iff \dim(\mathcal{Z}_N) - \dim(\mathcal{U}_M) \leqslant \dim(\mathcal{Z}_N \cap \mathcal{U}_M^\perp) \\ &\implies 1 \leqslant \dim(\mathcal{Z}_N \cap \mathcal{U}_M^\perp) \\ &\iff \mathcal{Z}_N \cap \mathcal{U}_M^\perp \neq \{0\} \\ &\iff \beta_{N,M} = 0, \end{aligned}$$

where the last equivalence follows from Proposition 3.

In practice, the matrices $\mathbf{A}$ and $\mathbf{B}$ are computed using the algebraic formulas $\mathbf{A} = \mathbf{U}_M\mathbf{M}\mathbf{U}_M$, and $\mathbf{B} = \mathbf{Z}_N\mathbf{M}\mathbf{U}_M$, where $\mathbf{M}$ is the Gram matrix of the inner product in $\mathcal{U}$. Thus, solving (18) allows for a straightforward reconstruction of the components of the state estimate in the basis of $\mathcal{U}^{\mathcal{N}}$ as follows:

$$\boldsymbol{u}^*_{N,M} = \mathbf{Z}_N\boldsymbol{z}^*_{N,M} + \mathbf{U}_M\boldsymbol{\eta}^*_{N,M}. \tag{23}$$

Offline/online procedure: Since several realizations $u^{\text{true}}(\omega)$ of the true state are considered, an offline/online procedure can be employed. During the offline stage, one precomputes the RB functions $(\zeta_n)_{1\leqslant n\leqslant N}$ and the Riesz representers $(q_m)_{1\leqslant m\leqslant M}$ leading to the matrices $\mathbf{A} \in \mathbb{R}^{M\times M}$ and $\mathbf{B} \in \mathbb{R}^{N\times M}$ once and for all. Then, during the online stage, for each new set of observations corresponding to a new realization of the true state $u^{\text{true}}(\omega)$, all that remains to be performed is to form the vector of observations $\boldsymbol{\ell}^{\text{obs}}_M(\omega)$ and to retrieve the deduced background estimate $\boldsymbol{z}^*_{N,M}(\omega)$ and the update estimate $\boldsymbol{\eta}^*_{N,M}(\omega)$ by solving the $(N+M)$-dimensional linear problem (18). The PBDW state estimate $\boldsymbol{u}^*_{N,M}(\omega)$ is then computed using (23).

Remark 4 (Choice of spaces)**.** *The subspaces $\mathcal{Z}_N$ and $\mathcal{U}_M$ must be chosen carefully. In fact, we want a small angle between the spaces $\mathcal{Z}_N$ and $\mathcal{U}_M$ in order to increase the stability constant, but we need some overlap between the spaces $\mathcal{Z}_N^\perp$ and $\mathcal{U}_M$ to improve the approximation capacity of $\mathcal{Z}_N^\perp \cap \mathcal{U}_M$. We refer the reader to [1] for a detailed a priori error analysis and to [17] for an overview on the influence of the spaces $\mathcal{Z}_N$ and $\mathcal{U}_M$ on the accuracy of the results.*

3 Time-dependent PBDW

Consider a finite time interval $I = [0, T]$, with $T > 0$. To discretize in time, we consider an integer $K \geqslant 1$, we define $0 = t^0 < \cdots < t^K = T$ as $(K + 1)$ distinct time nodes over I, and we set $\mathbb{K}^{\text{tr}} = \{1, \ldots, K\}$, $\overline{\mathbb{K}}^{\text{tr}} = \{0\} \cup \mathbb{K}^{\text{tr}}$ and $I^{\text{tr}} = \{t^k\}_{k\in\overline{\mathbb{K}}^{\text{tr}}}$. This section aims at deriving a state estimate for a time-dependent solution in the framework illustrated in 3.

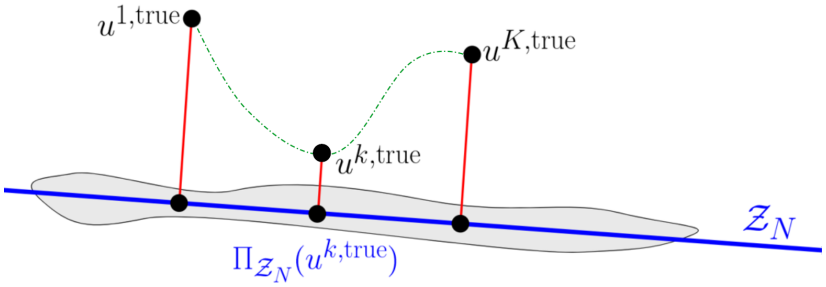

Figure 3: Characterization of the `bk` model in a time-dependent context.

Remark 5 (Initial condition)**.** *In the present setting, we choose not to solve the PBDW statement for the initial time node $k = 0$. It is straightforward to consider a setting where the initial time node is also included.*

3.1 Unlimited-observations statement

In this ideal setting, we assume that $u^{\text{true}} \in \mathcal{C}^0(I;\mathcal{U})$. The time-dependent unlimited-observations PBDW statement reads: for each $k \in \mathbb{K}^{\text{tr}}$, find $(u_N^{k,*}, z_N^{k,*}, \eta_N^{k,*}) \in \mathcal{U} \times \mathcal{Z}_N \times \mathcal{U}$ such that

$$(u_N^{k,*}, z_N^{k,*}, \eta_N^{k,*}) = \underset{\substack{u_N\in\mathcal{U}\\ z_N\in\mathcal{Z}_N\\ \eta_N\in\mathcal{U}}}{\operatorname{arginf}} \|\eta_N\|^2, \tag{24}$$

subject to

$$(u_N, v) = (\eta_N, v) + (z_N, v), \qquad \forall v \in \mathcal{U}, \tag{25a}$$
$$(u_N, \phi) = (u^{k,\text{true}}, \phi), \qquad \forall \phi \in \mathcal{U}. \tag{25b}$$

where $u^{k,\text{true}} := u^{\text{true}}(t^k, \cdot)$. For each $k \in \mathbb{K}^{\text{tr}}$, the solution of (24)-(25) is given by

$$u_N^{k,*} = u^{k,\text{true}}, \quad z_N^{k,*} = \Pi_{\mathcal{Z}_N}(u^{k,\text{true}}), \quad \eta_N^{k,*} = \Pi_{\mathcal{Z}_N^\perp}(u^{k,\text{true}}). \tag{26}$$

The Euler–Lagrange saddle-point problem associated with the time-dependent PBDW statement (24)-(25) reads: for each $k \in \mathbb{K}^{\text{tr}}$, find $(z_N^{k,*}, \eta_N^{k,*}) \in \mathcal{Z}_N \times \mathcal{U}$ such that

$$(\eta_N^{k,*}, q) + (z_N^{k,*}, q) = (u^{k,\text{true}}, q), \quad \forall q \in \mathcal{U}, \tag{27a}$$
$$(\eta_N^{k,*}, p) = 0, \qquad \forall p \in \mathcal{Z}_N. \tag{27b}$$

The unlimited-observations state estimate is then

$$u_N^{k,*} = z_N^{k,*} + \eta_N^{k,*}, \quad \forall k \in \mathbb{K}^{\text{tr}}. \tag{28}$$

3.2 Limited-observations statement

We now weaken the regularity assumption on the true state and only assume that $u^{\text{true}} \in L^1(I;\mathcal{U})$. We introduce the time-integration intervals

$$\mathcal{I}^k = [t^k - \delta t_k, t^k + \delta t_k], \quad \forall k \in \mathbb{K}^{\text{tr}}, \tag{29}$$

where $\delta t^k > 0$ is a parameter related to the precision of the sensor (ideally, $\delta t^k < \min(t^{k+1} - t^k, t^k - t^{k-1})$ with obvious adaptation if k=K). Then, for any function $v \in L^1(I;\mathcal{U})$, we define the time-averaged snapshots

$$v^k(x) := \frac{1}{|\mathcal{I}^k|} \int_{\mathcal{I}^k} v(t,x)\, dt \in \mathcal{U}, \quad \forall k \in \mathbb{K}^{\text{tr}}. \tag{30}$$

As in the steady case, we consider observation functionals that render the behavior of given sensors. We use the same observation functionals as in the time-independent setting, but we let them act on the time-averaged snapshots of the true solution, i.e., we consider

$$\ell_m^{k,\text{obs}}(u^{\text{true}}) := \ell_m^{\text{obs}}(u^{k,\text{true}}), \quad \forall m \in \{1,\dots,M\},\ \forall k \in \mathbb{K}^{\text{tr}}. \tag{31}$$

For instance, if the sensors act through local uniform time integration (see (7)), we have

$$\ell_m^{k,\text{obs}}(u^{\text{true}}) = \frac{1}{|\mathcal{R}_m|} \int_{\mathcal{R}_m} u^{k,\text{true}}(x)\, dx = \frac{1}{|\mathcal{R}_m|} \frac{1}{|\mathcal{I}_k|} \int_{\mathcal{R}_m} \int_{\mathcal{I}_k} u^{\text{true}}(t,x)\, dxdt, \tag{32}$$

whereas if the sensors act through integration against a Gaussian (see (8)), we have

$$\begin{aligned} \ell_m^{k,\text{obs}}(u^{\text{true}}) &= \frac{1}{\sqrt{2\pi r_m^2}} \int_{\mathcal{R}_m} u^{k,\text{true}}(x) \exp\left(\frac{-(x - x_m^c)^2}{2r_m^2}\right) dxdt, \\ &= \frac{1}{|\mathcal{I}_k|} \frac{1}{\sqrt{2\pi r_m^2}} \int_{\mathcal{I}_k} \int_{\mathcal{R}_m} u^{\text{true}}(x) \exp\left(\frac{-(x - x_m^c)^2}{2r_m^2}\right) dxdt. \end{aligned} \tag{33}$$

Generally, we introduce the time-independent observable space $\mathcal{U}_M \subset \mathcal{U}$ such that

$$\mathcal{U}_M = \text{Span}\{q_1, \dots, q_M\}. \tag{34}$$

The observation functionals in $\mathcal{U}'$ are then defined as

$$\ell_m^{k,\mathrm{obs}}(u^{\mathrm{true}}) = (u^{k,\mathrm{true}}, q_m), \quad \forall m \in \{1,\dots,M\}, \quad \forall k \in \mathbb{K}^{\mathrm{tr}}. \tag{35}$$

Note that, for fixed sensor locations, the computational effort to compute the Riesz representations of the observation functionals is time-independent and is incurred only once so that the experimental observations of the true state satisfy

$$\ell_m^{k,\mathrm{obs}}(u^{\mathrm{true}}) = \left(u^{k,\mathrm{true}}, q_m\right) = \frac{1}{|\mathcal{I}_k|}\int_{\mathcal{I}^k} \ell_m^{\mathrm{obs}}(u^{\mathrm{true}}(t,\cdot))dt, \ \forall m \in \{1,\dots,M\}, \ \forall k \in \mathbb{K}^{\mathrm{tr}}. \tag{36}$$

Hence, for all $q \in \mathcal{U}_M$ such that,

$$q = \sum_{m=1}^{M} \alpha_m q_m, \tag{37}$$

the inner product $\left(u^{k,\mathrm{true}}, q\right)$ is deduced from the experimental observations as follows:

$$\left(u^{k,\mathrm{true}}, q\right) = \frac{1}{|\mathcal{I}_k|}\int_{\mathcal{I}^k} \sum_{m=1}^{M} \alpha_m \left(u^{\mathrm{true}}(t,\cdot), q_m\right) dt = \frac{1}{|\mathcal{I}_k|}\sum_{m=1}^{M} \alpha_m \int_{\mathcal{I}^k} \ell_m^{\mathrm{obs}}(u^{\mathrm{true}}(t,\cdot))dt. \tag{38}$$

We are now ready to write the limited-observations PBDW statement: for each $k \in \mathbb{K}^{\mathrm{tr}}$, find $(u_{N,M}^{k,*}, z_{N,M}^{k,*}, \eta_{N,M}^{k,*}) \in \mathcal{U} \times \mathcal{Z}_N \times \mathcal{U}$ such that

$$(u_{N,M}^{k,*}, z_{N,M}^{k,*}, \eta_{N,M}^{k,*}) = \underset{\substack{u_{N,M}\in\mathcal{U}\\ z_{N,M}\in\mathcal{Z}_N\\ \eta_{N,M}\in\mathcal{U}}}{\operatorname{arginf}} \ \|\eta_{N,M}\|^2, \tag{39}$$

subject to

$$(u_{N,M}, v) = (\eta_{N,M}, v) + (z_{N,M}, v), \qquad \forall v \in \mathcal{U}, \tag{40a}$$
$$(u_{N,M}, \phi) = (u^{k,\mathrm{true}}, \phi), \qquad \forall \phi \in \mathcal{U}_M. \tag{40b}$$

The limited-observations saddle-point problem associated with (39) reads: for each $k \in \mathbb{K}^{\mathrm{tr}}$, find $(z_{N,M}^{k,*}, \eta_{N,M}^{k,*}) \in \mathcal{Z}_N \times \mathcal{U}_M$ such that

$$(\eta_{N,M}^{k,*}, q) + (z_{N,M}^{k,*}, q) = (u^{k,\mathrm{true}}, q), \quad \forall q \in \mathcal{U}_M, \tag{41a}$$
$$(\eta_{N,M}^{k,*}, p) = 0, \qquad \forall p \in \mathcal{Z}_N, \tag{41b}$$

and the limited-observations state estimate is

$$u_{N,M}^{k,*} = z_{N,M}^{k,*} + \eta_{N,M}^{k,*}, \quad \forall k \in \mathbb{K}^{\mathrm{tr}}. \tag{42}$$

Remark 6 (Pointwise measurements)**.** *For simplicity of implementation, assuming that* $u^{\mathrm{true}} \in \mathcal{C}^0(I;\mathcal{U})$*, one may consider pointwise measurements in time, i.e.,*

$$\left(u^{k,\mathrm{true}}, q_m\right) = \ell_m^{\mathrm{obs}}(u^{\mathrm{true}}(t^k,\cdot)), \quad \forall m \in \{1,\dots,M\}, \forall k \in \mathbb{K}^{\mathrm{tr}}. \tag{43}$$

The assumption (43) *is typically reasonable for a sensor of small precision* δt^k*.*

In algebraic form, the limited-observations PBDW statement reads: for each $k \in \mathbb{K}^{\mathrm{tr}}$, find $(\boldsymbol{z}^{k,*}, \boldsymbol{\eta}^{k,*}) \in \mathbb{R}^N \times \mathbb{R}^M$ such that

$$\begin{pmatrix} \mathbf{A} & \mathbf{B} \\ \mathbf{B}^T & \mathbf{0} \end{pmatrix} \begin{pmatrix} \boldsymbol{\eta}^{k,*} \\ \boldsymbol{z}^{k,*} \end{pmatrix} = \begin{pmatrix} \boldsymbol{\ell}^{k,\mathrm{obs}} \\ \mathbf{0} \end{pmatrix}, \tag{44}$$

with the matrices

$$\mathbf{A} = \Big((q_{m'}, q_m)\Big)_{1\leqslant m,m'\leqslant M} \in \mathbb{R}^{M\times M},\ \mathbf{B} = \Big((\zeta_n, q_m)\Big)_{1\leqslant m\leqslant M, 1\leqslant n\leqslant N} \in \mathbb{R}^{M\times N}, \tag{45}$$

and the vector of observations

$$\boldsymbol{\ell}^{k,\mathrm{obs}} = \big(\ell_m^{\mathrm{obs}}(u^{k,\mathrm{true}})\big)_{1\leqslant m\leqslant M} \in \mathbb{R}^M. \tag{46}$$

Similarly to the steady PBDW linear system (18), we solve (44) through an offline/online decomposed computational procedure whenever several realizations $u^{\mathrm{true}}(\omega)$ of the true state are to be considered.

Remark 7 (PBDW matrices)**.** *Notice that the PBDW matrices* $\mathbf{A}$ *and* $\mathbf{B}$ *are time-independent; only the right-hand side in* (44) *depends on* k*.*

4 Offline stage

In this section, we discuss the offline stage. Our main goal is to address the construction of the background space $\mathcal{Z}_N$.

4.1 Background space construction via `POD-greedy`

Suppose that we have computed a set of HF trajectories

$$\mathcal{S} = (\mathcal{S}_k)_{k\in\mathbb{K}^{\mathrm{tr}}} = \big((u^k(\mu))_{\mu\in\mathcal{P}^{\mathrm{tr}}}\big)_{k\in\mathbb{K}^{\mathrm{tr}}}, \tag{47}$$

where $u^k(\mu) := u(\mu)(t^k, \cdot)$, for all $k \in \mathbb{K}^{\mathrm{tr}}$. If we were to consider the PBDW statement (39)-(40) for each $k \in \mathbb{K}^{\mathrm{tr}}$ as an independent steady PBDW statement, we would be working with the time-dependent background spaces

$$\mathcal{Z}_{N^k}^k = \mathtt{POD}(\mathcal{S}_k, \epsilon_{\mathrm{POD}}), \quad \forall k \in \mathbb{K}^{\mathrm{tr}}, \tag{48}$$

where the procedure `POD` is defined in Chapter 1. However, this strategy is not convenient since the sizes N^k of the background spaces $\mathcal{Z}_{N^k}^k$ would depend on k. Since the observable space $\mathcal{U}_M$ is fixed, the same non-homogeneity between time nodes would also arise in the stability constant $\beta_{N^k,M}$. Thus, we propose to apply a `POD-greedy` algorithm [18] in order to build a time-independent background space $\mathcal{Z}_N$ that will be used for all $k \in \mathbb{K}^{\mathrm{tr}}$. The advantage is that the PBDW matrices $\mathbf{A}$ and $\mathbf{B}$ and the stability constant $\beta_{N,M}$ remain unchanged regardless of the discrete time node. The offline stage using the `POD-greedy` algorithm is summarized in Algorithm 1.

Algorithm 1 Offline stage via `POD-greedy`

Input : $\mathcal{S}$ and ϵ_{POD}.
$\mathcal{Q}^{\mathrm{init}}$: an initial set of Riesz representations for the observations.

1: Compute $\mathcal{Z}_N := \mathtt{POD\text{-}greedy}(\mathcal{S}, \epsilon_{\mathrm{POD}})$.
2: Set $\mathcal{U}_M := \mathrm{Span}\{\mathcal{Q}^{\mathrm{init}}\}$.
3: Compute the matrices $\mathbf{A}$ and $\mathbf{B}$ using $\mathcal{Z}_N$ and $\mathcal{U}_M$.

Output : $\mathcal{Z}_N$, $\mathcal{U}_M$, $\mathbf{A}$ and $\mathbf{B}$.

4.2 Background space construction via state estimation

We now devise a new algorithm in the context of time-dependent PBDW to perform the offline stage. Here, the construction of the background space $\mathcal{Z}_N$, the choice of the observation space $\mathcal{U}_M$ and the PBDW matrices are modified. The key idea of the new procedure is to precompute the PBDW state estimates of the parameters in the training set $\mathcal{P}^{\text{tr}}$ during the offline stage. The background space is then deduced from these PBDW state estimates. The benefit is that the newly created background space incorporates data-based knowledge. The modified offline stage of the PBDW for time-dependent problems is described in Algorithm 2. Within the modified offline stage, we use the so-called 'Greedy stability maximization' (`S-Greedy`) algorithm (considered in [1]) in line 6 in order to identify the least stable mode and then take the best measurement. The algorithm uses an input space $\mathcal{Z}_N$ that results from a `POD-greedy` procedure so that $\mathcal{Z}_1$ contains the dominant mode, and so forth. The `S-greedy` algorithm selects the observations progressively. Thus, the enrichment of the observable space $\mathcal{U}_M$ stops once the minimum stability β_{MIN} is reached. The procedure `S-greedy` is described in Algorithm 3 below. Altogether, the modified offline stage in the proposed algorithm

Algorithm 2 Modified offline stage of the time-dependent PBDW

Input : $\mathcal{P}^{\text{tr}}$, $\mathbb{K}^{\text{tr}}$, $\mathcal{S}$, ϵ_{POD}, $\epsilon_{\text{POD}}^{\text{init}}$ and β_{MIN}.
$\mathcal{Q}^{\text{init}}$: an initial set of Riesz representations of observations.

1: Compute $\mathcal{Z}_{N^{\text{init}}}^{\text{init}} :=$ `POD-greedy`$(\mathcal{S}, \epsilon_{\text{POD}}^{\text{init}})$.
2: Set $\mathcal{U}_{M^{\text{init}}}^{\text{init}} := \text{Span}\{\mathcal{Q}^{\text{init}}\}$.
3: Compute the matrices $\mathbf{A}^{\text{init}}$ and $\mathbf{B}^{\text{init}}$ using $\mathcal{Z}_{N^{\text{init}}}^{\text{init}}$ and $\mathcal{U}_{M^{\text{init}}}^{\text{init}}$.
4: Estimate the state $u^{k,*}(\mu)$ for all $(\mu, k) \in \mathcal{P}^{\text{tr}} \times \mathbb{K}^{\text{tr}}$.
5: Compute $\mathcal{Z}_N :=$ `POD-greedy`$(\{u^{k,*}(\mu)\}_{\mu \in \mathcal{P}^{\text{tr}}, k \in \mathbb{K}^{\text{tr}}}, \epsilon_{\text{POD}})$.
6: Compute $\mathcal{U}_M :=$ `S-Greedy`$(\mathcal{P}^{\text{tr}}, \mathbb{K}^{\text{tr}}, N, \{\mathcal{Z}_n\}_{n=1}^{N}, \beta_{\text{MIN}}, \mathcal{Q}^{\text{init}})$.
7: Compute the matrices $\mathbf{A}$ and $\mathbf{B}$ using $\mathcal{Z}_N$ and $\mathcal{U}_M$.

Output : $\mathcal{Z}_N$, $\mathcal{U}_M$, $\mathbf{A}$ and $\mathbf{B}$.

offers four major advantages:

1. **Improved background space:** Since the background space $\mathcal{Z}_N$ is built using both the `bk` model and the observations, it is expected to have better approximation capacities of the true state.

2. **Reduced number of online observations:** In line 6 of Algorithm 2, we select each new data point so as to maximize the stability constant $\beta_{N,M}$. Thus, the observations that will be used during the online stage are mainly needed only for stability and not for accuracy.

3. **Reduced dimension of the online PBDW statement:** Since the number of observations is significantly reduced, the modified PBDW matrices are of smaller size compared to the matrices of the standard PBDW. Thus, using the modified offline algorithm, the online PBDW formulation is solved faster.

4. **Reduced storage cost:** Owing to the reduced number of online measurements, the dimensions of the observable space $\mathcal{U}_M$ and of the matrices $\mathbf{A}$ and $\mathbf{B}$ are smaller, whence the storage gain.

Regarding computational efficiency, the modified procedure consists of more steps than in the standard PBDW. However, all the additional steps of the algorithm are performed offline. As for all reduced-order modeling techniques, the goal of the algorithm is to further improve the online efficiency. Hence, the computational savings brought by the new PBDW formulation come, in our

Algorithm 3 `S-Greedy`: Stability-maximization algorithm

Input : N, $\mathcal{Z}_N$ and $\beta_{\text{MIN}} \in (0,1]$.
$\mathcal{Q}^{\text{init}}$: an initial set of Riesz representations of the observations.

1: Choose a random $q_1 \in \mathcal{Q}^{\text{init}}$.
2: Set $\mathcal{U}_1 := \text{Span}\{q_1\}$.
3: Compute the stability constant $\beta_{1,1}$ using $\mathcal{Z}_1$ and $\mathcal{U}_1$.
4: Set $m := 2$.
5: **while** $\beta_{N,m-1} < \beta_{\text{MIN}}$ or $m < M$ **do**
6: Compute the least stable mode and the associated supremizer

$$w_{\text{inf}} \in \underset{w \in \mathcal{Z}_N}{\text{arginf}} \sup_{v \in \mathcal{U}_{m-1}} \frac{(w,v)}{\|w\| \, \|v\|}, \quad \text{and} \quad v_{\text{sup}} = \Pi_{\mathcal{U}_{m-1}}(w_{\text{inf}}).$$

7: Identify the least well-approximated vector $q_m = \underset{q \in \mathcal{Q}^{\text{init}}}{\text{argsup}} \, |(q, w_{\text{inf}} - v_{\text{sup}})|$.
8: Set $\mathcal{U}_m := \text{Span}\{\mathcal{U}_{m-1}, q_m\}$.
9: Compute the stability constant $\beta_{N,m}$.
10: $m = m + 1$.
11: **end while**
12: $M := m$.

Output : $\mathcal{U}_M$.

opinion, at a reasonable offline price. Indeed, the resolution of the (online) standard PBDW statement for each parameter $\mu \in \mathcal{P}^{\text{tr}}$ has a reduced computational cost. The only relevant additional computational cost incurred offline is related to the second `POD-greedy` algorithm (cf. line 5 of Algorithm 2). We believe this computational effort remains acceptable.

Remark 8 (Least stable mode)**.** *Line 6 of Algorithm 3 may return several infima. Among these infima, we select a function whose norm in $\mathcal{U}$ is maximal.*

Remark 9 (Steady setting)**.** *In a time-dependent framework, the computational savings induced by the modified offline stage are substantial, in particular because of the influence of the time steps. However, Algorithm 3 can be applied in the steady setting as well.*

5 Numerical results

In this section, we illustrate the above developments on test cases related to the heat equation. The goal is to illustrate the computational performance of our algorithms. In all our test cases, we consider a two-dimensional setting based on the plate illustrated in the left panel of Figure 4 with $\Omega = (-2,2)^2 \subset \mathbb{R}^2$. We use a finite element subspace $\mathcal{U}^{\mathcal{N}} \subset \mathcal{U} = H^1(\Omega)$ consisting of continuous, piecewise affine functions in order to generate HF trajectories. The FEM subspace $\mathcal{U}^{\mathcal{N}}$ is based on a mesh that contains $\mathcal{N} = 6561$ nodes. The experimental data is generated synthetically and the observation subsets $\{\mathcal{R}_m\}_{1 \leqslant m \leqslant M}$ are uniformly selected over the plate as illustrated in the left panel of Figure 4. Regarding the implementation, the HF computations use the software `FreeFem++` [20], whereas the reduced-order modeling and the PBDW-related algorithms have been developed in `Python`.

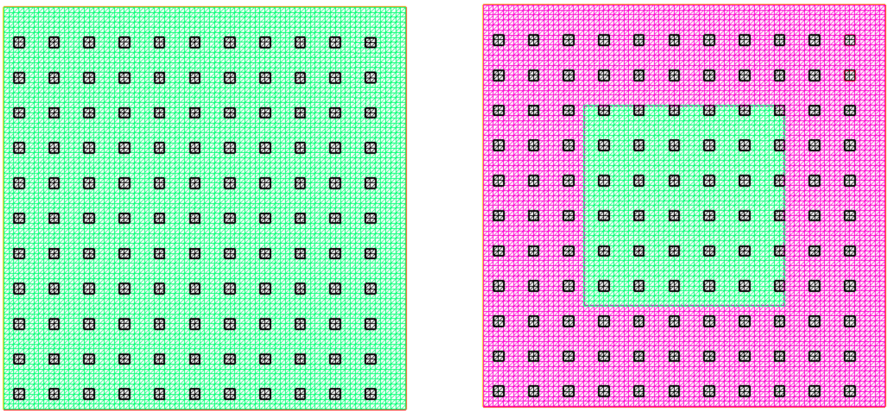

Figure 4: Computational domain and mesh with $\mathcal{N} = 6561$. The little black squares are observation subsets $\{\mathcal{R}_m\}_{m=1}^{121}$. Left: Mono-material plate. Right: Bi-material plate.

5.1 Physical model problem

We apply the above methodology to the following parabolic PDE: For many values of the parameter $\mu \in \mathcal{P}$, find $u(\mu) : I \times \Omega \to \mathbb{R}$ such that

$$\begin{cases} \dfrac{\partial u(\mu)}{\partial t} - \nabla \cdot (D(\mu)\nabla u(\mu)) = 0, & \text{in } I \times \Omega, \\ u(\mu)(t = 0, \cdot) = u_0, & \text{in } \Omega, \\ \text{Boundary conditions}, & \text{on } I \times \partial\Omega, \end{cases} \tag{49}$$

where $u_0 = 293.15\text{K}$ (20^oC). We will supplement (49) with two types of boundary conditions:

1. **Linear heat equation:** We apply a homogeneous Neumann boundary condition on $\partial\Omega_0$ and a non-homogeneous Neumann boundary condition on $\partial\Omega_n$, i.e.,

$$\begin{cases} -D(\mu)\dfrac{\partial u(\mu)}{\partial n} = 0, & \text{on } I \times \partial\Omega_0, \\ -D(\mu)\dfrac{\partial u(\mu)}{\partial n} = \phi_e, & \text{on } I \times \partial\Omega_n, \end{cases} \tag{50}$$

   with $\phi_e = 3\text{K}{\cdot}\text{m}{\cdot}\text{s}^{-1}$, $\partial\Omega_0 = (-2, 2) \times \{2\} \cup \{2\} \times (-2, 2)$, and $\partial\Omega_n = (-2, 2) \times \{-2\} \cup \{-2\} \times (-2, 2)$. Thus, the resulting problem (49)−(50) is linear. Note that $\partial\Omega_0$ consists of the upper and right sides of the plate and $\partial\Omega_n$ consists of its lower and left sides, so that $\partial\Omega = \overline{\partial}\Omega_0 \cup \overline{\partial}\Omega_n$.

2. **Nonlinear heat equation:** We apply Stefan–Boltzmann boundary conditions on $\partial\Omega$, i.e.,

$$-D(\mu)\frac{\partial u}{\partial n} = \sigma\varepsilon(u^4 - u_r^4), \qquad \text{on } I \times \partial\Omega, \tag{51}$$

   where $u_r = 303.15\text{K}$ (30^oC) is an enclosure temperature, $\sigma = 5.67 \times 10^{-8}\text{W.m}^{-2}\text{.K}^{-4}$ is the Stefan–Boltzmann constant and $\varepsilon = 3.10^{-3}$ is the emissivity. The Stefan–Boltzmann boundary condition is nonlinear and so is the resulting problem (49)−(51).

In what follows, the background spaces $\mathcal{Z}_N$ will be generated by solving either the linear PDE (49)−(50) or the nonlinear PDE (49)−(51) with a uniform diffusivity function $D(\mu)$ such that for all $x \in \Omega$, $D(\mu)(x) = D_{\text{uni}}(\mu)(x) := \mu\mathbf{1}_\Omega(x)$.

5.2 Synthetic data generation

We synthesize the data by first synthesizing a true solution and then applying to it the linear functionals by means of their Riesz representations in the observable space $\mathcal{U}_M$. In order to synthesize the true solution, we consider a 'true model' based on the bi-material plate (cf. right panel of Figure 4) where we choose a fixed internal diffusivity $D_{\text{int}} = 1$ and define, for each $\mu \in \mathcal{P}$, the diffusivity function $D(\mu)$ as $D(\mu)(x) = D_{\text{syn}}(\mu)(x) := \mu D_{\text{int}} \mathbf{1}_{\Omega_{\text{ext}}}(x) + D_{\text{int}} \mathbf{1}_{\Omega_{int}}(x)$, for all $x \in \Omega$, where $\Omega_{\text{int}} = (-1, 1)^2$ and $\Omega_{\text{ext}} = (-2, 2)^2 \backslash (-1, 1)^2$, so that $\overline{\Omega} = \overline{\Omega}_{\text{int}} \cup \overline{\Omega}_{\text{ext}}$ and $\Omega_{\text{int}} \cap \Omega_{\text{ext}} = \varnothing$. The synthetic true solutions are then defined as the solutions of (49) for all $\mu \in \mathcal{P}$, with either the linear boundary condition (50) or the nonlinear boundary condition (51).

5.2.1 Test configurations

In order to investigate the PBDW formulation, we perform test cases on two distinct configurations:

1. **Perfect model:** The `bk` model is said to be perfect when $\epsilon^{\text{bk}}_{\text{mod}}(u^{\text{true}}(\omega)) = 0$, for every $\omega \in \Theta$ (see (1)) (we recall that ω represents the unanticipated uncertainty). In this situation, $u^{\text{true}}(\omega) \in \mathcal{M}^{\text{bk}}$ for all $\omega \in \Theta$. Although the model is perfect, some discrepancies between the HF solutions and the measurements might arise from model-order reduction since $\mathcal{M}^{\text{bk}} \neq \mathcal{Z}_N$ (cf. Figure 1). Note that this scenario seldom occurs in engineering situations. This test configuration is meant to assess the accuracy of the PBDW formulation when the observable space $\mathcal{U}_M$ scarcely has additional information compared to $\mathcal{Z}_N$.

2. **Imperfect model:** The `bk` model is said to be imperfect when the modeling error does not vanish. In this situation, there exists at least one (and in general many) $\omega \in \Theta$ such that $\epsilon^{\text{bk}}_{\text{mod}}(u^{\text{true}}(\omega)) \neq 0$, i.e., $u^{\text{true}}(\omega) \notin \mathcal{M}^{\text{bk}}$. Consider for instance the plates in Figure 4. If the true solution is generated synthetically using the bi-material plate, an example of an imperfect `bk` model can be the one for which we solve the same PDE that has generated the true states without accounting for the difference in diffusivity between the subdomains of the plate.

5.3 Background space construction via `POD-greedy`

In this section, four test cases are considered to study the PBDW approach.

- Test case (a): Linear perfect.
- Test case (b): Linear imperfect.
- Test case (c): Nonlinear perfect.
- Test case (d): Nonlinear imperfect.

5.3.1 Linear case

Regarding time discretization, we consider the time interval $I = [0, 10]$s, the set of discrete times nodes $\mathbb{K}^{\text{tr}} = \{1, \ldots, 200\}$, and a constant time step $\Delta t^k = 0.05$s for all $k \in \mathbb{K}^{\text{tr}}$. Finally, we introduce the parameter interval $\mathcal{P} = [0.05, 1]$ and the training set $\mathcal{P}^{\text{tr}} = 0.05 \times \{1, \ldots, 20\}$. In Figure 5, we show the HF temperature profiles for the model problem (49)−(50) over the homogeneous plate at the end of the simulation, i.e., for $t^K = 10$s and for two parameter values. We recall that these solutions will be used as true solutions for the perfect linear case. As the time evolves, the energy related to the flux ϕ_e propagates through the plate which is progressively heated. Moreover, the overall temperature is higher for smaller values of the parameter μ than for larger values. As physically expected, the thermal diffusion over the plate is stronger for larger values of μ than for smaller values.

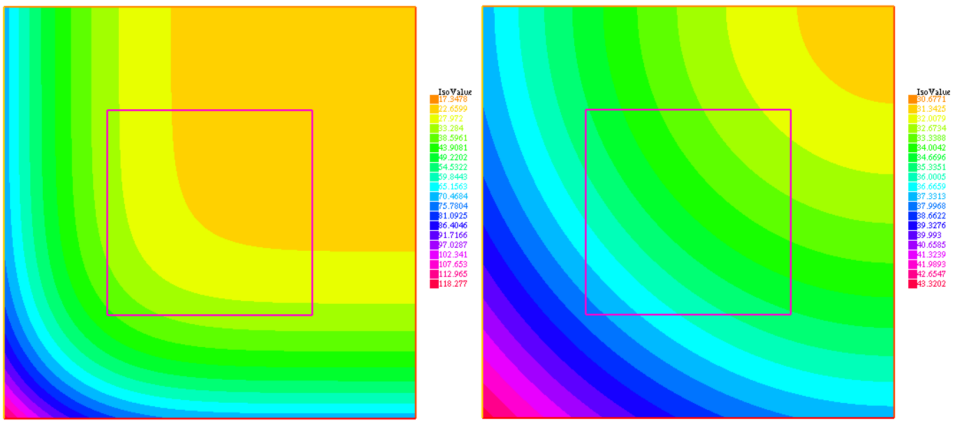

Figure 5: Test cases (a) and (b) : HF solutions for the `bk` model with Neumann boundary conditions. Left: $\mu = 1$ in D_{uni} (values from 17.3^{o}C to 118.3^{o}C). Right: $\mu = 20$ in D_{uni} (values from 30.7^{o}C to 43.3^{o}C).

Test case (a): Linear perfect model We consider the case of a perfect `bk` model for which the diffusivity is uniform over the entire domain Ω. Thus, the true solutions correspond to the HF computations of the `bk` model. The resulting trajectories are reduced using the `POD-greedy` algorithm. For instance, for a tolerance value $\epsilon_{\text{POD}} = 10^{-2}$, the background space $\mathcal{Z}_N$ is composed of $N = 5$ modes. Regarding observations, the initial set $\mathcal{Q}^{\text{init}}$ is obtained using $M = \text{Card}(\mathcal{Q}^{\text{init}}) = 121$ sensors that are uniformly placed over the plate (see Figure 4). Using both the background space $\mathcal{Z}_N$ and the observable space $\mathcal{U}_M(\mathcal{Q}^{\text{init}})$, we build the offline matrices $\mathbf{A}$ and $\mathbf{B}$. During the online stage, we estimate the state $u^*_{N,M}$ for every parameter μ in the training set $\mathcal{P}^{\text{tr}}$. Using the weighted H^1-norm, the state estimation relative H^1-error $e^k(\mu)$ defined as

$$e^k(\mu) := \frac{\|u^{k,\text{true}}(\mu) - u^{k,*}_{N,M}(\mu)\|_{H^1(\Omega)}}{\|u^{k,\text{true}}(\mu)\|_{H^1(\Omega)}}, \quad \forall \mu \in \mathcal{P}, \tag{52}$$

is displayed in Figure 6 as a function of the value of the parameter μ for several values of ϵ_{POD}. In

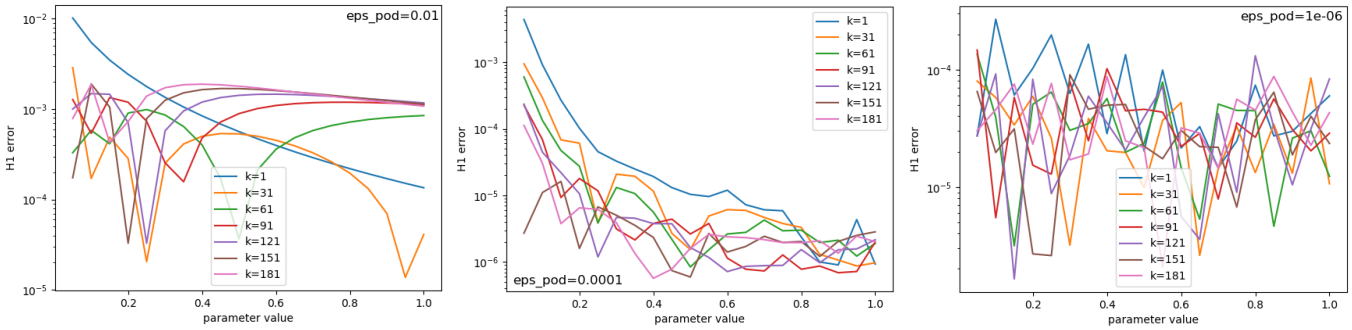

Figure 6: Test case (a): Relative H^1-error $e^k(\mu)$ for some time nodes $k \in \mathbb{K}^{\text{tr}}$. Left: $\epsilon_{\text{POD}} = 10^{-2}$ ($N = 5$). Middle : $\epsilon_{\text{POD}} = 10^{-4}$ ($N = 10$). Right: $\epsilon_{\text{POD}} = 10^{-6}$ ($N = 15$).

this first configuration, one can notice that the error decreases for smaller tolerances ϵ_{POD}, i.e., with the dimension N of the background space $\mathcal{Z}_N$. However, the bottom-right panel of Figure 6 shows a starting increase in the relative H^1-error $e^k(\mu)$ for $\epsilon_{\text{POD}} = 10^{-6}$ and an oscillatory behavior of the relative H^1-error $e^k(\mu)$. Although counter-intuitive in the reduced-basis context, this phenomenon is due to the deterioration of the stability constant $\beta_{N,M}$. This observation confirms the claims made in Remark 4.

Test case (b): Linear imperfect model This second test investigates the case of a linear imperfect `bk` model. In Figure 7, we show the HF temperature profiles for the true solutions over

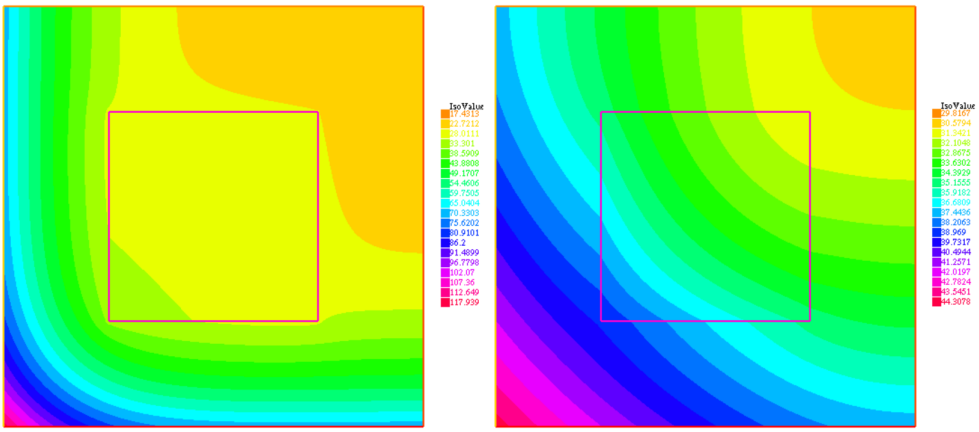

Figure 7: Test case (b) : Synthetic true solutions with Neumann boundary conditions. Left: $\mu = 1$ in $D_{\text{syn}}(\mu)$ (values from 17.4^{o}C to 117.9^{o}C). Right: $\mu = 20$ in $D_{\text{syn}}(\mu)$ (values from 29.8^{o}C to 44.3^{o}C).

the bi-material plate at the end of the simulation, i.e., at $t^K = 10$s and for two different parameter values. The temperature fields exhibit the same overall behavior as in Figure 5. Additionally, we notice that the difference in diffusivity between Ω_{int} and Ω_{ext} leads as expected to a kink in the temperature isolines. When $\mu < 1$, the thermal diffusion is stronger in the inner plate corresponding to Ω_{int}, whereas for $\mu > 1$, the thermal diffusion is weaker in the inner plate. Using the HF trajectories produced by the `bk` model, we generate a background space $\mathcal{Z}_N$ by means of a `POD-greedy` algorithm. We use $M = 121$ observations to build the observable space $\mathcal{U}_M$. The relative H^1-errors $e^k(\mu)$ defined in (52) are shown in Figure 8 as a function of the value of the parameter μ. For instance, for a tolerance value $\epsilon_{\text{POD}} = 10^{-3}$, $\mathcal{Z}_N$ is spanned by $N = 7$ vectors. Notice that the error vanishes for $\mu = 0.5$ since this configuration is equivalent to a perfect `bk` model. However, the bottom panels of Figure 8 show a gradual error increase with the dimension N of the `bk` space. This tendency was already observed for the linear perfect test case, although in smaller proportions. As before, the stability constant $\beta_{N,M}$ is degraded when increasing the dimension N of the background space $\mathcal{Z}_N$. Moreover, the enrichment of $\mathcal{Z}_N$ does not add relevant modes anymore (in terms of associated singular values). For the sake of comparison, we enrich the observable space $\mathcal{U}_M$ such that $M = 676$ and plot the relative H^1-errors $e^k(\mu)$ for the same values of ϵ_{POD} in Figure 9. Our interpretation is confirmed since the stability issues do not arise anymore for $\epsilon_{\text{POD}} = 10^{-4}$. Owing to the increase of M, the stability decrease with respect to N is somewhat compensated. Finally, the bottom-right panel of Figure 9 shows the beginning of an error increase. Using the same reasoning as above, we conclude that more observations are needed for $\epsilon_{\text{POD}} = 10^{-6}$.

Finally, we visualize the stability constant $\beta_{N,M}$ as a function of the number of observations M in Figure 10. The left panel of the figure shows a single curve for clarity, whereas the right panel includes curves for several values of the tolerance ϵ_{POD} (note that the two panels do not use the same rule). As expected, for a constant value of N, the more the observations, the better the stability. For a number of observations $M = 3000$, the PBDW formulation is perfectly stable (or close to) for all the considered values of ϵ_{POD}.

5.3.2 Nonlinear case

Here, we consider the PDE (49)−(51) with $u_r = 303.15$K, $\sigma = 5.67 \times 10^{-8}$W.m^{-2}.K^{-4} and $\varepsilon = 3.10^{-3}$. Except for the parameter interval $\mathcal{P} = [0.1, 2]$, the set $\mathcal{P}^{\text{tr}} = \{0.1i, 1 \leqslant i \leqslant 20\}$ and the time step

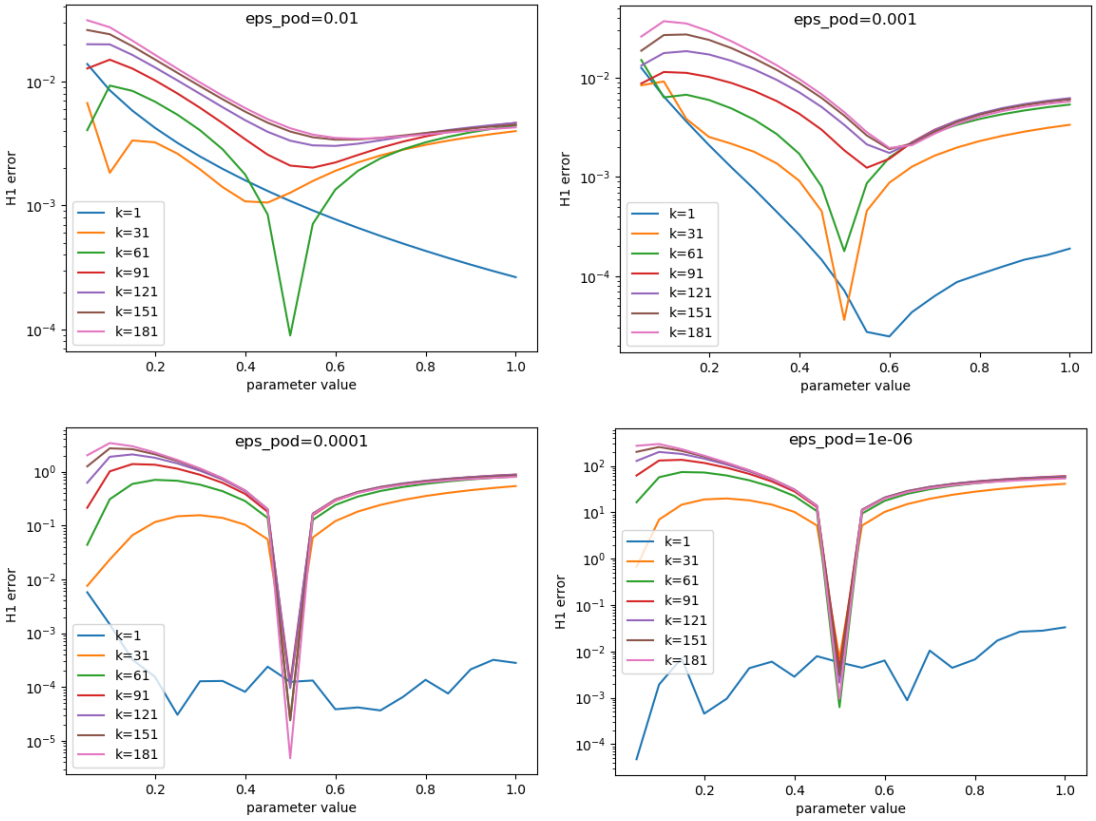

Figure 8: Test case (b) : Relative H^1-error $e^k(\mu)$ for some time nodes $k \in \mathbb{K}^{\text{tr}}$ and $M = 121$. Top left: $\epsilon_{\text{POD}} = 10^{-2}$ ($N = 5$). Top right: $\epsilon_{\text{POD}} = 10^{-3}$ ($N = 7$). Bottom left: $\epsilon_{\text{POD}} = 10^{-4}$ ($N = 10$). Bottom right: $\epsilon_{\text{POD}} = 10^{-6}$ ($N = 15$).

$\Delta t^k = 0.1$, all the other numerical data remain the same as for the linear test case from the previous section.

5.3.3 Test case (c): Nonlinear perfect model

We consider the case with a perfect `bk` model. Thus, the true solutions correspond to the HF computations of the `bk` model (cf. left panel of Figure 11). The resulting trajectories are reduced using the `POD-greedy` algorithm. For instance, for a tolerance value $\epsilon_{\text{POD}} = 10^{-2}$, the background space $\mathcal{Z}_N$ consists of $N = 3$ modes. Regarding observations, the initial set $\mathcal{Q}^{\text{init}}$ is obtained using $M = \text{Card}(\mathcal{Q}^{\text{init}}) = 121$ sensors that are uniformly placed over the plate (see Figure 4). During the online stage, we estimate the state $u^*_{N,M}$ for every parameter μ in the training set $\mathcal{P}^{\text{tr}}$. In Figure 12, we display the state estimation relative H^1-error $e^k(\mu)$ defined in (52) as a function of the value of the parameter μ for several values of ϵ_{POD}. In contrast to the linear case, the error always decreases for smaller tolerances ϵ_{POD}, i.e., with the dimension N of the background space $\mathcal{Z}_N$. However, we expect that, for some very small tolerance value (e.g. ϵ_{POD} such that $N > M$), the stability issues mentioned above would arise again.

5.3.4 Test case (d): Nonlinear imperfect model

This test case investigates a nonlinear imperfect `bk` model for which the HF `bk` solutions and the true solutions are respectively displayed in the left and right panels of Figure 11. The temperature profile for the true solution over the bi-material plate at the end of the simulation, i.e., at $t^K = 10$s clearly shows a different behavior at the boundaries of the inner material. Regarding the PBDW state estimation, Figure 13 shows the relative H^1-error $e^k(\mu)$ defined in (52) using $M = 121$ observations to build the observable space $\mathcal{U}_M$. For $\epsilon_{\text{POD}} = 10^{-4}$, $\mathcal{Z}_N$ is spanned by $N = 7$ vectors. Notice that

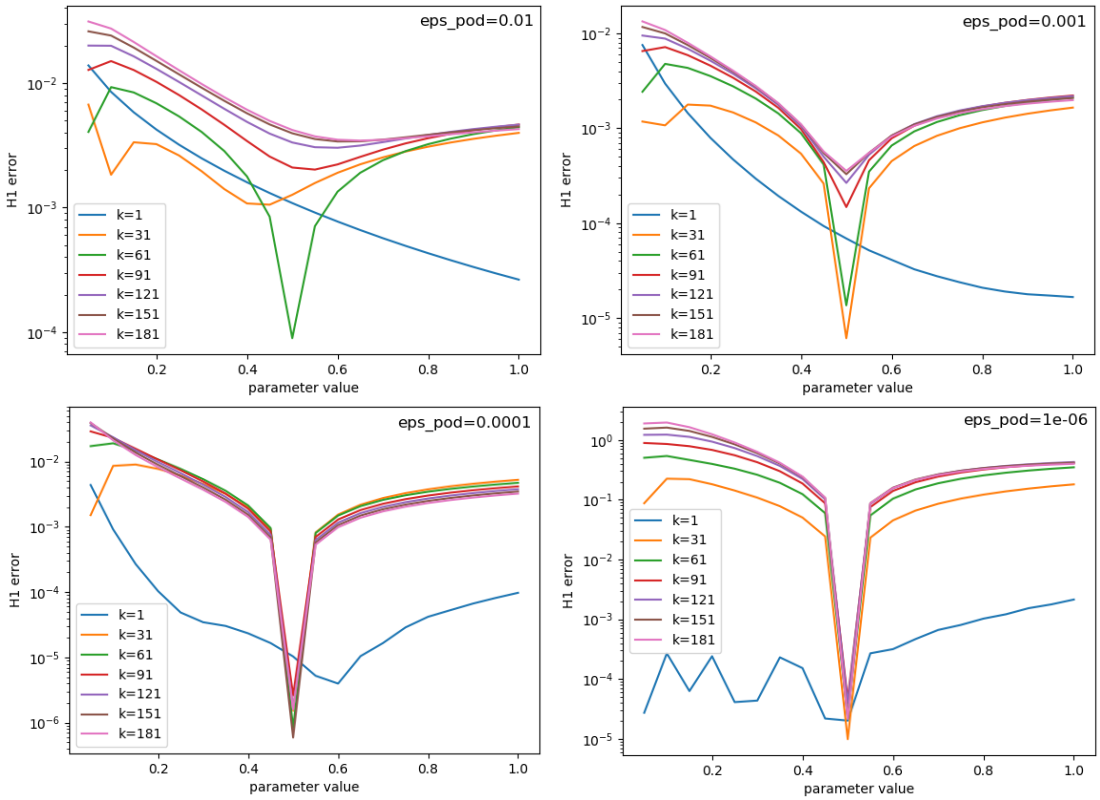

Figure 9: Test case (b) : Relative H^1-error $e^k(\mu)$ for some time nodes $k \in \mathbb{K}^{\text{tr}}$ and $M = 676$. Top left: $\epsilon_{\text{POD}} = 10^{-2}$ ($N = 5$). Top right: $\epsilon_{\text{POD}} = 10^{-3}$ ($N = 7$). Bottom left: $\epsilon_{\text{POD}} = 10^{-4}$ ($N = 10$). Bottom right: $\epsilon_{\text{POD}} = 10^{-6}$ ($N = 15$).

the error vanishes for $\mu = 0.25$ since this configuration is equivalent to a perfect `bk` model. We notice that the relative H^1-error $e^k(\mu)$ increases because the stability constant decreases. Figure 14 visualizes the relative H^1-error $e^k(\mu)$ for a higher number of observations $M = 676$. We observe that augmenting the dimension of the observable space $\mathcal{U}_M$ cures the stability issues. Also, the errors are lower owing to the higher number of observations. Finally, Figure 15 shows the stability constant $\beta_{N,M}$ as a function of the number of observations M. The behavior is quite similar to the linear case. Hence, the nonlinear character of the problem does not influence the overall features of the PBDW statement. This observation corroborates the independence with regard to the `bk` model.

5.4 Background space construction via state estimation

We now illustrate the performances of Algorithm 2 for the following linear imperfect case:

- Test case (e): We consider a simulation duration $T = 4$s and a time step $\Delta t = 0.1$s. Test truths are synthesized with an internal diffusivity $D_{\text{int}} = 0.2$.

As opposed to the previous section, we choose a non-parametric `bk` model based on an HF computation for $\mu = 0.5$. The resulting unique trajectory is then reduced using a `POD` algorithm, which is equivalent to a `POD-greedy` for a single trajectory (cf. line 1 of Algorithm 2). For a tolerance value $\epsilon_{\text{POD}}^{\text{init}} = 10^{-2}$, we obtain a background space $\mathcal{Z}_{N^{\text{init}}}^{\text{init}}$ composed of $N^{\text{init}} = 34$ modes. As regards observations, the initial set $\mathcal{Q}^{\text{init}}$ consists of $M^{\text{init}} = \text{Card}(\mathcal{Q}^{\text{init}}) = 1521$ sensors that are uniformly placed over the plate (cf. line 2 of Algorithm 2). Using both the background space $\mathcal{Z}_{N^{\text{init}}}^{\text{init}}$ and the observable space $\mathcal{U}_{M^{\text{init}}}^{\text{init}}(\mathcal{Q}^{\text{init}})$, we estimate the state $u^*_{N^{\text{init}},M^{\text{init}}}$ for every parameter μ in the training set $\mathcal{P}^{\text{tr}} = \{0, 4, 8, 12, 16\}$ (cf. line 4 of Algorithm 2). The state estimation leads to the relative H^1-error $e^k(\mu)$ shown in Figure 16. We also plot in Figure 17 the absolute H^1-norms of the deduced

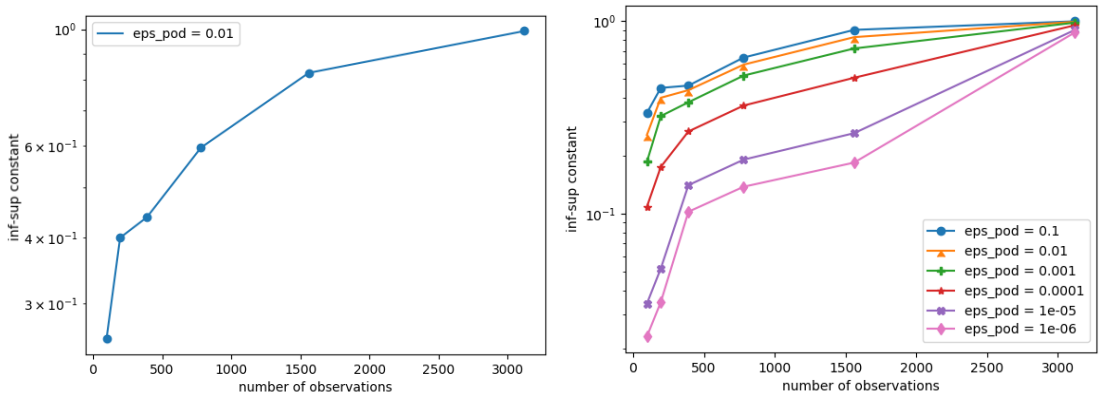

Figure 10: Test case (b) : Stability constant $\beta_{N,M}$ as a function of M. On the right panel, the values of N are respectively 3, 5, 7, 10, 13, 15 for the values of ϵ_{POD} in decreasing order.

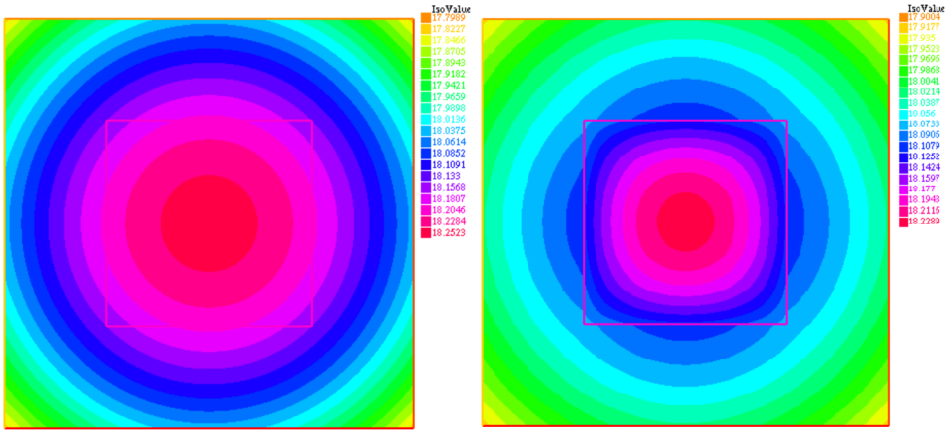

Figure 11: Test cases (c) and (d) : Left: HF solution for the `bk` model (values from 17.80^{o}C to 18.25^{o}C). Right: Synthetic true solution using a bi-material plate (values from 17.90^{o}C to 18.23^{o}C).

background estimate $z^*_{N^{\text{init}},M^{\text{init}}}$ and the update estimate $\eta^*_{N^{\text{init}},M^{\text{init}}}$. One can notice that the latter is non-negligible compared to the former. Once the first part of the modified offline stage has been performed, we use the resulting state estimates in order to build the modified background space (cf. line 5 of Algorithm 2). For a tolerance $\epsilon_{\text{POD}} = 5.10^{-2}$, the `POD-greedy` algorithm selects four modes. Then, we build the observable space $\mathcal{U}_M$ using $M = 121$ uniformly distributed sensors (the optimal choice can be made using the `S-Greedy` algorithm, see Algorithm 3). Figure 18 displays the errors for the verification set $\mathcal{P}^{\text{verif}} = \{0, \ldots, 19\}$. The state estimation relative H^1-error $e^k(\mu)$ remains comparable to that of the five parameters used for the offline construction. Regarding the online observations, we highlight that the online results are achieved using only $M \approx 8\% M^{\text{init}}$. Finally, Figure 19 shows the absolute H^1-norms of the deduced background estimate $z^*_{N,M}$ and the update estimate $\eta^*_{N,M}$. We observe that the update estimate $\eta^*_{N,M}$ has a lower norm compared to Figure 17, whereas the deduced background estimate $z^*_{N,M}$ has a larger norm. This is due to the offline inclusion of observations in the new background space $\mathcal{Z}_N$ through offline state estimation. Therefore, we deduce that the modified offline algorithm achieves the expected objective.

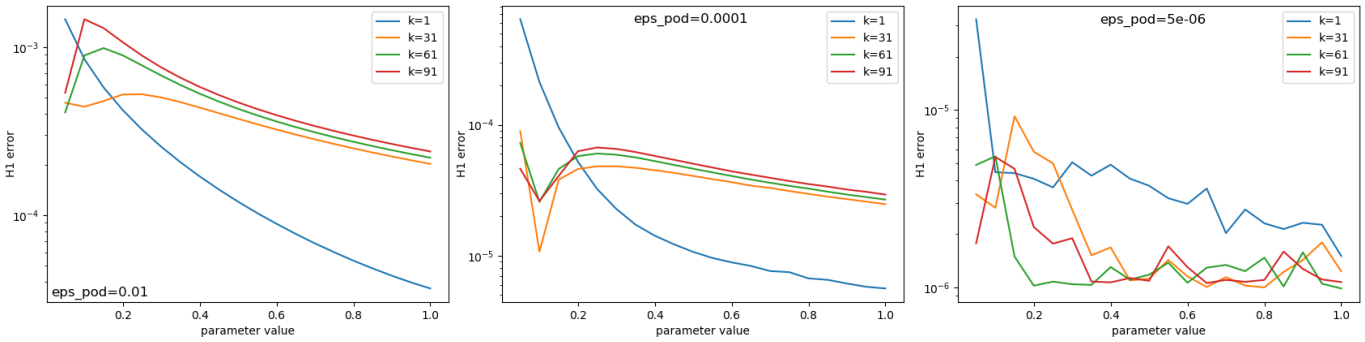

Figure 12: Test case (c) : Relative H^1-error $e^k(\mu)$ for some time nodes $k \in \mathbb{K}^{\text{tr}}$ and $M = 121$. Left: $\epsilon_{\text{POD}} = 10^{-2}$ $(N = 3)$. Middle: $\epsilon_{\text{POD}} = 10^{-4}$ $(N = 7)$. Right: $\epsilon_{\text{POD}} = 5.10^{-6}$ $(N = 11)$.

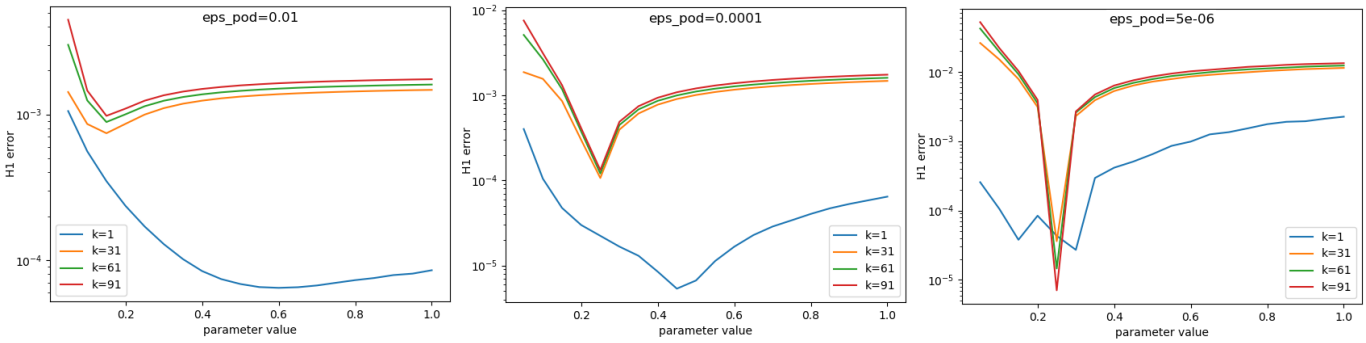

Figure 13: Test case (d) : Relative H^1-error $e^k(\mu)$ for some time nodes $k \in \mathbb{K}^{\text{tr}}$ and $M = 121$. Left: $\epsilon_{\text{POD}} = 10^{-2}$ $(N = 3)$. Middle: $\epsilon_{\text{POD}} = 10^{-4}$ $(N = 7)$. Right: $\epsilon_{\text{POD}} = 10^{-6}$ $(N = 11)$.

6 Conclusion and perspectives

We have presented a time-dependent extension of the PBDW approach with a modified offline stage that suits both the stationary and time-dependent cases. As regards the time-dependent setting, numerical tests on both linear and nonlinear cases assess the efficiency of the method for well chosen dimensions of the `bk` space $\mathcal{Z}_N$ and of the observable space $\mathcal{U}_M$. The test cases show that augmenting the dimension N of $\mathcal{Z}_N$ is counter-productive starting from a certain rank due of the deterioration of the stability constant $\beta_{N,M}$. In such cases, increasing the dimension of the observable space $\mathcal{U}_M$ is an alternative that restores a good stability of the problem. However, the measurements are expensive to obtain in engineering scenarios. In this context, a modified offline stage is introduced so as to reduce the number of final observations that are required within the online stage. The numerical performances obtained produce accuracy levels that are comparable to the standard method. A promising application is the assessment of the proposed methodology in three-dimensional industrial cases. Another interesting research direction is the inclusion of noise in the time-dependent framework.

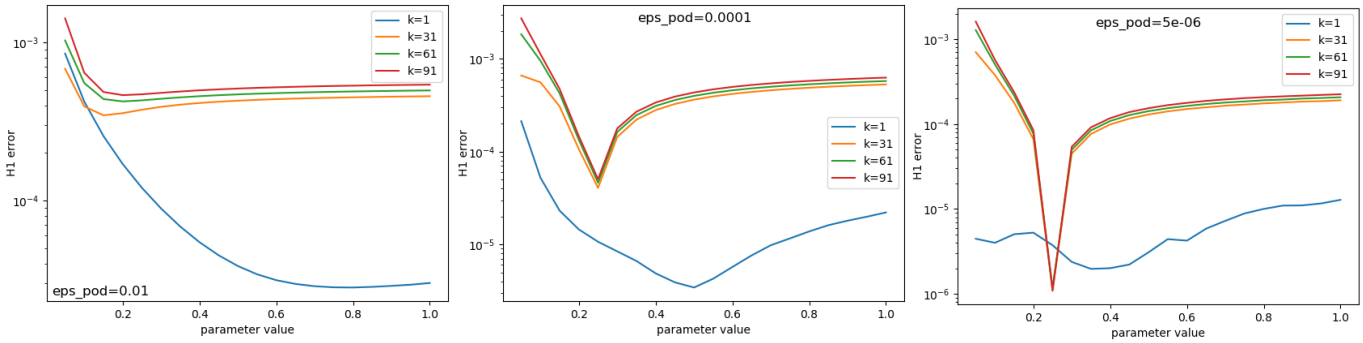

Figure 14: Test case (d) : Relative H^1-error $e^k(\mu)$ for some time nodes $k \in \mathbb{K}^{\text{tr}}$ and $M = 676$. Left: $\epsilon_{\text{POD}} = 10^{-2}$ $(N = 3)$. Middle: $\epsilon_{\text{POD}} = 10^{-4}$ $(N = 7)$. Right: $\epsilon_{\text{POD}} = 5.10^{-6}$ $(N = 11)$.

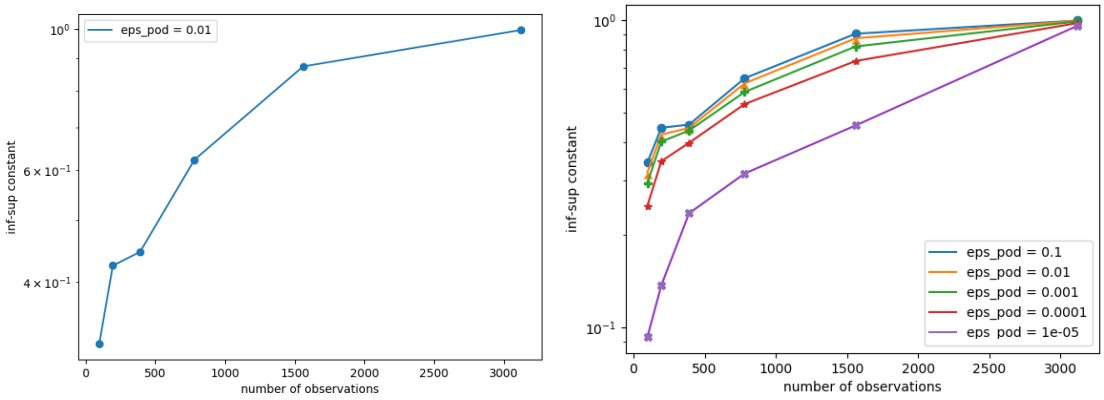

Figure 15: Test case (d) : Stability constant $\beta_{N,M}$. On the right panel, the values of N are respectively 2, 3, 5, 7, 11 for the values of ϵ_{POD} in decreasing order.

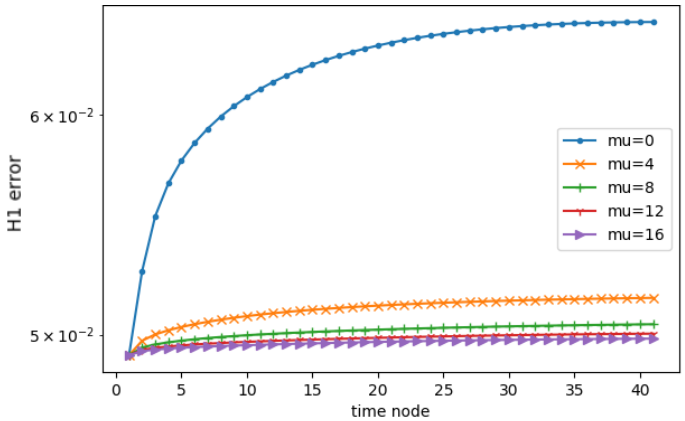

Figure 16: Test case (e) : Relative H^1-error $e^k(\mu)$ for the state estimate as a function of the time nodes. The curves correspond to different values of μ.

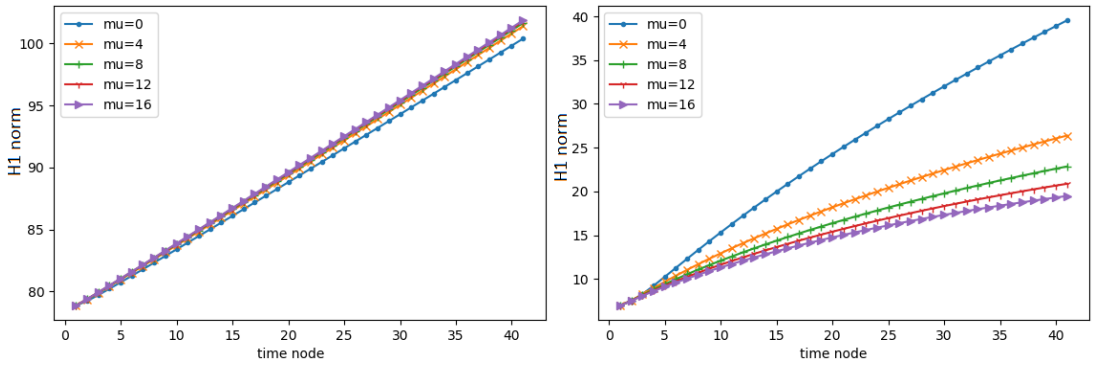

Figure 17: Test case (e) : Absolute H^1-norms of the contributions $z^*_{N^{\text{init}},M^{\text{init}}}$ and $\eta^*_{N^{\text{init}},M^{\text{init}}}$ as a function of the time nodes. The various curves correspond to the different values of μ.

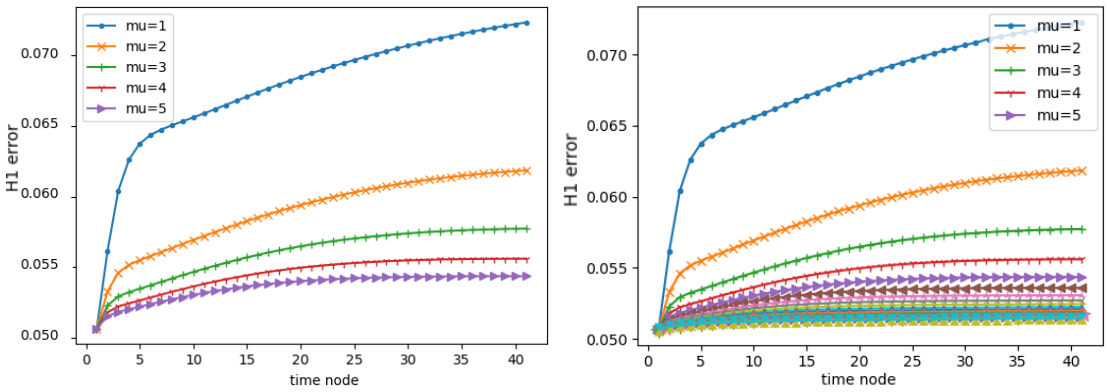

Figure 18: Test case (e) : Relative H^1-error $e^k(\mu)$ for the state estimate as a function of the time nodes during the online stage. The various curves correspond to the different values of μ. Left: for all $\mu \in \mathcal{P}^{\text{tr}}$. Right: for all $\mu \in \mathcal{P}^{\text{verif}}$.

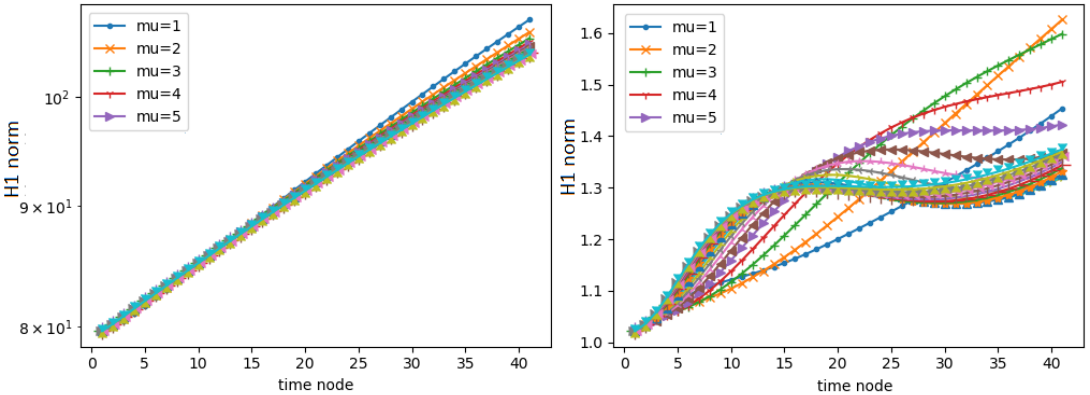

Figure 19: Test case (e) : Absolute H^1-norms of the contributions $z^*_{N,M}$ and $\eta^*_{N,M}$ as a function of the time nodes. The various curves correspond to the different values of μ.

References

[1] Y. Maday, A. T. Patera, J. D. Penn, and M. Yano, "A parameterized-background data-weak approach to variational data assimilation: formulation, analysis, and application to acoustics," *Internat. J. Numer. Methods Engrg.*, vol. 102, no. 5, pp. 933–965, 2015.

[2] T. Taddei, J. D. Penn, M. Yano, and A. T. Patera, "Simulation-based classification; a model-order-reduction approach for structural health monitoring," *Arch. Comput. Methods Eng.*, vol. 25, no. 1, pp. 23–45, 2018.

[3] J. K. Hammond, R. Chakir, F. Bourquin, and Y. Maday, "PBDW: A non-intrusive Reduced Basis Data Assimilation method and its application to an urban dispersion modeling framework," *Appl. Math. Model.*, vol. 76, pp. 1–25, 2019.

[4] J.-P. Argaud, B. Bouriquet, F. de Caso, H. Gong, Y. Maday, and O. Mula, "Sensor placement in nuclear reactors based on the generalized empirical interpolation method," *J. Comput. Phys.*, vol. 363, pp. 354–370, 2018.

[5] J. P. Argaud, B. Bouriquet, H. Gong, Y. Maday, and O. Mula, "Stabilization of (G)EIM in presence of measurement noise: application to nuclear reactor physics," in *Spectral and high order methods for partial differential equations—ICOSAHOM 2016*, vol. 119 of *Lect. Notes Comput. Sci. Eng.*, pp. 133–145, Springer, Cham, 2017.

[6] Y. Maday and O. Mula, "A generalized empirical interpolation method: application of reduced basis techniques to data assimilation," in *Analysis and numerics of partial differential equations*, vol. 4 of *Springer INdAM Ser.*, pp. 221–235, Springer, Milan, 2013.

[7] Y. Maday, O. Mula, A. Patera, and M. Yano, "The generalized empirical interpolation method: Stability theory on hilbert spaces with an application to the stokes equation," *Computer Methods in Applied Mechanics and Engineering*, vol. 287, pp. 310 – 334, 2015.

[8] Y. Maday, O. Mula, and G. Turinici, "Convergence analysis of the generalized empirical interpolation method," *SIAM J. Numer. Anal.*, vol. 54, no. 3, pp. 1713–1731, 2016.

[9] Y. Maday, A. T. Patera, J. D. Penn, and M. Yano, "PBDW state estimation: noisy observations; configuration-adaptive background spaces; physical interpretations," in *CANUM 2014—42e Congrès National d'Analyse Numérique*, vol. 50 of *ESAIM Proc. Surveys*, pp. 144–168, EDP Sci., Les Ulis, 2015.

[10] Y. Maday and T. Taddei, "Adaptive PBDW Approach to State Estimation: Noisy Observations; User-Defined Update Spaces," *SIAM J. Sci. Comput.*, vol. 41, no. 4, pp. B669–B693, 2019.

[11] F. Galarce, J.-F. Gerbeau, D. Lombardi, and O. Mula, "State estimation with nonlinear reduced models. Application to the reconstruction of blood flows with Doppler ultrasound images," *arXiv e-prints*, p. arXiv:1904.13367, Apr 2019.

[12] H. Gong, Y. Maday, O. Mula, and T. Taddei, "PBDW method for state estimation: error analysis for noisy data and nonlinear formulation," *arXiv e-prints*, p. arXiv:1906.00810, Jun 2019.

[13] T. Taddei, J. D. Penn, and A. T. Patera, "Validation by Monte Carlo sampling of experimental observation functionals," *Internat. J. Numer. Methods Engrg.*, vol. 112, no. 13, pp. 2135–2150, 2017.

[14] T. Taddei and A. T. Patera, "A localization strategy for data assimilation; application to state estimation and parameter estimation," *SIAM J. Sci. Comput.*, vol. 40, no. 2, pp. B611–B636, 2018.

[15] A. Cohen, W. Dahmen, R. DeVore, J. Fadili, O. Mula, and J. Nichols, "Optimal reduced model algorithms for data-based state estimation," *arXiv e-prints*, p. arXiv:1903.07938, Mar 2019.

[16] P. Binev, A. Cohen, O. Mula, and J. Nichols, "Greedy algorithms for optimal measurements selection in state estimation using reduced models," *SIAM/ASA Journal on Uncertainty Quantification*, vol. 6, no. 3, pp. 1101–1126, 2018.

[17] A. Benaceur, *Model reduction for nonlinear problems in thermics and mechanics*. Thesis, Université Paris-Est Marne la Vallée, 2018.

[18] B. Haasdonk, "Convergence rates of the POD-greedy method," *ESAIM Math. Model. Numer. Anal.*, vol. 47, no. 3, pp. 859–873, 2013.

[19] A. Ern and J.-L. Guermond, *Theory and practice of finite elements*, vol. 159 of *Applied Mathematical Sciences*. Springer-Verlag, New York, 2004.

[20] F. Hecht, "New developments in freefem++." Open source on `http://www.freefem.org`, 2012.